To be published as a Chapter in 'Treatise
on Materials Science and Technology,"
R. K. MacCrone, Editor, Academic Press

LBL-4156
c. 1

DIRECT OBSERVATION AND CHARACTERIZATION OF DEFECTS IN MATERIALS

R. Sinclair

September 1975

Prepared for the U. S. Energy Research and
Development Administration under Contract W-7405-ENG-48

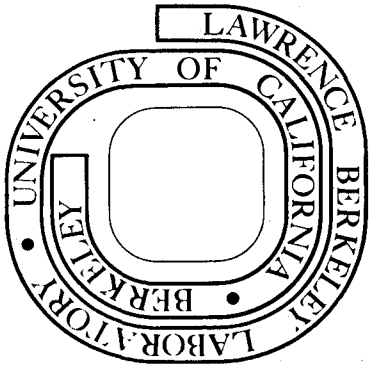

LBL-4156
c. 1

DISCLAIMER

LBL-4156

DIRECT OBSERVATION AND CHARACTERIZATION OF DEFECTS IN MATERIALS

R. Sinclair

Department of Materials Science and Engineering and Inorganic Materials Research Division, Lawrence Berkeley Laboratory, University of California, Berkeley, California 94720

CONTENTS

DIRECT OBSERVATION AND CHARACTERIZATION OF DEFECTS IN MATERIALS

R. Sinclair

1. Introduction

The purpose of the present article is to examine various experimental techniques whereby structural information may be obtained directly about defects in materials. This is an important subject as the properties of perfect materials are modified by the faults that are present. In order to understand their resultant effects the defects must be characterized to as great a degree as possible, the procedures for which are rapidly expanding as more detailed information is required. Obviously in a short article it is impossible to cover in any detail the various techniques. The approach taken here is to emphasize two important factors: the contrast mechanism by which faults are detected and the resolution which is necessary to study them.

To indicate the optimum use of the many methods currently available, the characteristics of various faults are firstly discussed (section 2) together with the spatial scale over which they extend. Conventional methods of defect observation are then reviewed in section 3 and their appropriate applications outlined. Finally in section 4 a relatively recent development of transmission electron microscopy is described, the lattice or structure imaging technique. As this method possesses the capability of imaging the structure of most materials at the atomic level it may yield more valuable information than may be gathered by existing methods.

2. Lattice Defects

Most materials are crystalline and it is convenient to describe defects in terms of the lattice structure of crystals. They may be categorized according to the number of dimensions over which they extend (zero-dimensional, one dimensional etc.). The distortion of the crystal lattice generally occurs over a volume considerably greater than the actual center of the individual fault and thus information should be obtained not only at the core but also in areas far removed from it. The latter is more readily attainable except when ultra-high resolution techniques are applied. Figure 1 indicates the approximate sizes of the various faults.

There are several types of point or zero-dimensional defects: vacant lattice sites, self-interstitial atoms, substitutional solute atoms and interstitial solute atoms. Self point defects, being equilibrium defects, must always exist in a concentration dependent on the ambient temperature, unless a non-equilibrium concentration is introduced by quenching from a higher temperature or by knock-on displacement damage in a radiation environment. They are the smallest faults (of the order of atomic dimensions) and consequently are the most difficult to study directly. Their presence, however, can markedly affect atomic diffusion rates and hence time dependent processes in the solid state(e.g. precipitation, coarsening, creep); properties associated with regular crystalline periodicity can be modified (e.g. electrical, magnetic properties) and their lattice strain may alter mechanical properties and their interaction with other defects.

Dislocations in the lattice are the one-dimensional defects. Their

behaviour under stress provides the basis for the plasticity and toughness of metals and their presence may cause breakdown in electrical devices. Along the line of the fault they may extend considerable distances (e.g. the width of the crystal in which they exist) but perpendicular their dimensions are at the atomic level (see fig. 1). Thus information is more readily available about the dislocation lines rather than the distortions very close to the dislocation core.

Interfaces and stacking faults represent the two-dimensional lattice defects. These may be free surfaces, grain or crystal boundaries and interphase interfaces, with dimensions varying from small (~20Å x 20Å for small precipitate interfaces), medium (~100μ x 100μ for grain boundaries) to very large (~mms x mms for surfaces and cracks). They are relatively straightforward to detect although it is often the features which occur in the third dimension which most affect the properties of the material (and are the most difficult about which to obtain data). The three dimensional defects are voids, second phase particles and inclusions, and these also may exist over a wide range of scale (with small precipitates having a size of ~20Å, inclusions often being ~1μ and voids ranging from ~100Å to as large as ~1mm). The effect of two and three dimensional defects on properties is generally better understood as it is easier to correlate the associated modifications with these larger scale faults.

Information may be obtained on two levels; either about individual defects and their effect on the crystal lattice or about the mutual interaction and distribution of the faults. The latter is known as the <u>microstructure</u> of the material and it is often possible to identify the effects of various microstructures on the properties of

components. To observe the microstructure it is only necessary to detect, image and identify the appropriate faults which exist, which is an approach generally well-known to materials scientists. Details about their fine-scale structure is then generally not required. However, for a more sophisticated understanding of the effect of a particular fault a detailed characterization is necessary, often at the highest resolution possible. Thus there are two principal philosophies behind defect characterization of materials both of which are covered in the present article.

The range of use of the various investigative techniques is also shown in fig. 1. It can be seen that optical microscopy is sufficient for detail down to ~0.5μ , that scanning electron microscopy is appropriate for ~100Å detail but for extremely high resolution in which the atomic lattice itself may be resolved, transmission electron microscopy or field-ion microscopy are required.

3. Review of Investigative Techniques*

A. Optical Microscopy

In materials science the optical method is most often applied by reflection of light from the surface of the specimen. This surface is suitably prepared to reveal the microstructure of the material (e.g. by polishing and subsequent chemical etching). Contrast arises from the varying intensity of reflected light across the surface, which may be due to natural changes in reflectance caused by composition or structural

*For a more detailed account of the various experimental methods, see for instance Phillips (1971).

changes or by local changes of surface angle caused by preferential etching. A schematic example is shown in fig. 2. Various techniques such as polarized light microscopy, dark field microscopy etc. may be used to enhance contrast or to produce additional effects (Phillips, 1967, 1971). The ultimate resolution is limited by the wavelength of visible light and is normally given by the Rayleigh criterion:

$$\text{Resolution} = \frac{0.61\lambda}{\text{N.A.}}$$

where λ = wavelength and N.A. = numerical aperture.

As $\lambda \sim 0{,}5\mu$ and the maximum feasible aperture has N.A. ~ 1.4, it is not possible to reduce the resolution below about 0.2μ. The method is not applicable to gaining information about distortions in the atomic lattice, for detecting the fine scale defects such as vacancies or dislocations, unless they can be revealed by a large scale effect such as an etch pit (Thomas, 1973) nor for gaining crystallographic information. However, it is extremely useful for obtaining a low resolution view of microstructure and should precede more high resolution, specialist techniques to ensure that the appropriate level of examination is to be chosen. It has found a wide range of use in materials science in the past although the more detailed information currently required generally needs application of more sophisticated techniques.

A micrograph illustrating the application and limitation of optical microscopy is shown in fig. 3 taken of a Cu-Ni-Fe alloy aged at 840°C (Gronsky, 1974). The region where the interparticle spacing is larger than that in the surrounding material has been created by an enhanced precipitate coarsening at the grain boundary. This effect causes

intergranular embrittlement of the alloy, which otherwise could have a homogeneous and very desirable microstructure. The scale of this reaction is clearly shown by the micrograph but no information is given about whether a grain with a new orientation has been nucleated or whether grain boundary migration has occurred. This may be obtained by transmission electron microscopy and careful experimentation has shown the latter to be the case (Gronsky and Thomas, 1975). Thus information may be obtained about grain sizes, shape and the distribution of phases in a material, but not about their relative orientation nor about details on a scale finer than ~0.2-0.5μ.

B. Scanning Electron Microscopy (SEM)

Electrons possess several advantages over visible light in forming an image of an object. They are light, negatively charged particles a beam of which can be readily focussed by electromagnetic lenses. Their de Broglie wavelength, dependent on their energy, is considerably lower, being 0.122Å at 10keV and 0.037Å at 100keV. This imposes no limitation on the resolution of atoms (i.e. 2Å resolution), the minimum resolution being set by lens aberrations, microscope stability and the mode of image formation. Electron microscopy is thus preferable to optical microscopy for high resolution purposes.

In the scanning electron microscope an image is formed of the specimen surface by the use of a fine electron beam. (Thornton, 1968; Oatley, 1972; Hearle, Sparrow and Cross, 1972; Holt, Muir, Grant and Boswarva, 1974). Besides higher resolution several further advantages accrue from this technique. Firstly the depth of focus is increased by about three orders of magnitude owing to a narrow angle of

illumination. Secondly, the instrument may be used in a variety of operational modes by which different signals from the specimen can be processed. Thirdly, x-ray or electron signals induced from the specimen by the incident electron beam may be characterised to yield data on the local composition. Fourthly, crystallographic information may be obtained about the orientation from electron channeling patterns (Booker, 1970; Joy 1974) or about accurate local lattice parameters by use of Kossel patterns from emitted x-rays (Dingley and Steeds, 1974; Yakowitz, 1974).

The region near the specimen is shown schematically in fig. 4. The fine electron beam penetrates the sample to a depth of about a micron depending on the applied voltage and specimen material. Three emitted electron signals are produced. These are the high energy incident electrons which are back-scattered with no energy loss, low energy secondary electrons which can only escape from a region very close to the surface(within about 100Å) and the Auger electrons (Mac Donald , 1975) which have low energy characteristic of atoms in the area irradiated. These signals may be collected and processed separately. The incident beam is scanned across the specimen and the collected signal will vary in intensity in accordance with the particular features of the examined area. The signal is displayed in synchronization on a cathode-ray tube (CRT) so that an image is obtained of the total area scanned. The magnification achieved is simply the ratio of CRT area to the scanned area on the sample.

As an alternative to examining the emitted electron signal, the current passing through the sample to earth may be utilized in image

formation. Since this is the difference between the incident and emitted currents the contrast is readily interpretable. In studying semiconductor devices, a biassing voltage may also be applied to the specimen and the contrast from the specimen current utilised in plotting the current flow in the device. This application is an important diagnostic tool in the semiconductor industry. In addition, emitted electromagnetic radiation (x-rays, or visible light in the case of cathodoluminescent materials (Holt, 1974))can be used with suitable detectors to form the image. SEM is obviously an extremely versatile technique especially when one also considers instrumental variables such as applied voltage (5 - 50 kV) electron probe size, scanning speed, specimen tilt and collector angle. For in situ studies, hot, cold, deformation and environmental stages are available.

Contrast arises from the variation of the examined signal with the topography and chemical composition of the specimen surface. The most common operational mode in materials science is the emissive mode whereby the secondary emitted electrons are collected. The intensity of this signal is roughly proportional to sec θ (Oatley, 1972), where θ is the angle of beam incidence, and so the brightness of the image varies according to the local surface inclination. As only a small depth is examined, a picture is obtained of the specimen surface. The eye is sensitive to relatively small differences in brightness (and can detect the appropriate contrast) but is less sensitive to larger scale differences. Although the image may represent very large intensity differences from one region to another, the

eye reduces this to roughly what would be perceived from an optical micrograph of the surface under diffuse lighting conditions (Oatley, 1972). Thus we can interpret the image intuitively as we would a high magnification optical picture, with the contrast often being more marked (as in fig. 5). The considerably increased depth of field allows detailed examination of highly complex materials. This is also exemplified by fig. 5 in which it may be appreciated that even parts of the relatively flat expoxy matrix would be out of focus in an optical picture whereas the carbon fibres standing proud of the surface are quite dramatically shown in the scanning micrograph.

The intensity of the back-scattered electron beam varies with both inclination and average atomic number of the illuminated region (the secondary current is relatively insensitive to atomic number) so that by collecting these higher energy electrons information is obtained about both topography and chemical compositions. As the electrons come from a larger volume of material the clarity of the picture is reduced compared to the emissive mode. A polished specimen surface may be used for qualitative information in the image about composition alone. Conversely, the specimen current image (the difference between incident and total emitted currents) also yields information about both aspects of the sample.

It is evident that the resolution limit is set roughly by the probe size since the signal is processed from a region instantaneously irradiated by the electron beam. In commercial instruments possessing a tungsten, thermionic emission source this is about 100Å, reducing to about 50Å in the best circumstances (Broers, 1969). Although

further reduction in probe size is possible electron optically the commensurate decrease in image intensity makes recording times prohibitively long. A source with higher brightness can overcome this difficulty. Practical resolutions of ~25Å are expected for a lanthamum hexaboride emitter and a resolution of about 3Å may be achieved with a field-emission source (Muir, 1974; Crewe, 1974; Veneklasen, 1975). However, despite these possibilities, it is doubtful whether this resolution capability is desirable for scanning electron microscopes, especially when one considers the increased expense of the more refined systems. The primary purpose of the instrument is to view the surface of the specimen from which information may be obtained about the effect of the larger scale faults. Images may be formed in appropriate circumstances of the underlying finer scale defects such as dislocations and stacking faults (Clarke, 1971; Stern, Ichinokawa, Takashima, Hashimoto and Kimoto, 1972; Joy, Thompson, Booker and Andersen, 1974) but are inferior to those obtained by transmission electron microscopy. It would seem more worthwhile to utilize the technique in its optimum range (100Å - 100μ) rather than attempt to compete with transmission electron systems where the latter are superior.

In materials science SEM finds a widescale application, for instance in the study of fracture surfaces (e.g. fig. 6), eutectic and composite materials, electrodeposition and oxidation processes, sintering and complex three dimensional structures such as textile materials. The effect of magnetic fields on the emitted electrons allows contrast from magnetic domains and the effect of electrical fields permits

examination of semiconducting devices in operation. (For examples, see references in this section and also Lifshin, Morris and Bolon, 1969), the proceedings of the IIT conferences (Johari, 1968-1975) and for a bibliography Johnson 1975). It is an invaluable investigative tool, providing superior information to the optical microscope and complementary information to the transmission electron microscope.*

C. Transmission Electron Microscopy (TEM)

The principle of image formation in the transmission electron microscope involves magnifying the image produced in an electron beam which has passed through a thin foil specimen of the material. (Hirsch, Howie, Nicholson, Pashley and Whelan, 1965; Amelinckx, Gevers, Remaut and Van Landuyt, 1970; Thomas, Fulrath and Fisher, 1972; Glauert, 1972, 1974; Siegel and Beaman, 1975). The resolution depends on the stability of the lens and source voltage supply, mechanical stability of the microscope column, chromatic and spherical aberration (particularly of the objective lens which forms the first image of the sample). Currently available microscopes possess a guaranteed line resolution of $\lesssim$2Å with which it is possible to image atomic planes in alloys and individual atoms in ceramic materials. Micrographs can be taken in a magnification range of 10^2-10^6 times, overlapping with the effective scales of optical and scanning microscopy but also achieving atomic level resolution. Thus on the same specimen it is possible to characterize microstructure and to obtain detailed information about individual defects. Furthermore, the electron diffraction pattern of areas 1-100μ in diameter can be

* A comparison of the three techniques has been given by Hearle, 1972.

obtained in a straightforward manner to provide standard crystallographic data and to aid in the interpretation of the electron image. The technique is probably the most important one for the direct characterization of defects in materials.

There are three main modes of image formation (fig. 7):

(i) bright field imaging, whereby an aperture is positioned in the back focal plane of the objective lens to allow the electron beam transmitted through the sample to form the image;

(ii) dark field imaging, in which a beam diffracted by the crystal may be employed. This beam may be chosen by suitable positioning of the objective aperture but for highest resolution the illumination is tilted with respect to the specimen so that the diffracted beam is parallel to the optical axis of the microscope (fig. 7b);

(iii) lattice or structure imaging, which may be produced by allowing transmitted and diffracted beams to form the image using a suitably large objective aperture.

The diffraction pattern may be observed by focussing the microscope intermediate lens on the back focal plane of the objective lens rather than on the image plane.

Contrast arises from several sources. "Mass thickness" or "structure factor" contrast occurs owing to differing electron absorption in adjacent parts of the specimen. This is particularly useful in two-phase materials where chemical composition variations may cause corresponding variations of electron scattering power or may give rise to foil thickness variations by differential electropolishing behavior during sample preparation.

"Diffraction" contrast arises because the intensity of the transmitted and diffracted electron beams is altered locally near a defect. For instance if the specimen is oriented for high electron transmission (i.e. light area in bright field, dark in dark field) the lattice distortion caused by a dislocation may bring the atomic planes nearby into an orientation where strong diffraction can take place, with the Bragg condition locally satisfied. This region will appear dark against the bright background in the bright field image and vice versa in the dark field image. A dislocation line thus appears as a dark line in the TEM bright field image. A similar contrast mechanism operates for other lattice defects which give rise to lattice distortions (e.g. interstitial and vacancy loops, coherent precipitates). A grain boundary is readily recognised by changes of contrast arising from the different orientations of the adjacent crystals. Stacking faults produce contrast as the crystal periodicity is disturbed relative to surrounding perfect crystal and they appear as a series of fringes or dark lines parallel to the intersection of the fault with the specimen surface. Second phase particles are revealed by the mass thickness or structure factor contrast outlined above, but preferably they are studied in dark field by placing the aperture around a reflection originating from the second phase itself. Only the particles then appear bright in the dark field image. It is clear that one, two and three dimensional lattice defects readily produce characteristic contrast effects in TEM which can be studied at extremely high resolution (down to ~5Å). This is the principal reason why the technique

is so powerful for studying the microstructure of materials.

Interpretation of the precise contrast from lattice defects in TEM is a complex subject requiring detailed understanding of the dynamical theory of electron diffraction (see Hirsch et al. 1965, Brown, 1971). However, by systematic experimentation it is possible to uniquely identify the character of the fault. The habit of the fault (i.e. the line of a dislocation, the plane of a stacking fault or grain boundary, the shape of a precipitate) may be found by trace analysis, with the specimen orientation established from the diffraction pattern of the area of interest. A three-dimensional view of the microstructure may be obtained by a stereo pair of micrographs of the same area. The nature of the fault (e.g. Burger's vector of a dislocation, displacement vector of a stacking fault, misfit of a coherent particle) is found by a series of contrast experiments performed on the same area of the foil. The specimen is generally oriented close to "two beam diffracting conditions" (i.e. only one diffracted beam, $\underline{g}$, has high intensity and is close to the Bragg condition) and the behaviour of the defect image contrast in this and in a series of such diffracting conditons is carefully recorded. By suitable choice of $\underline{g}$ the character of the fault may be found. For example the Burger's vector ($\underline{b}$) of a dislocation may be determined by finding conditions under which the dislocation image disappears (or possesses weak contrast). This occurs when $\underline{g}.\underline{b} = 0$ i.e. the Burgers vector is perpendicular to the operating reflection. Figure 8 shows

the variation of contrast of interfacial dislocations in partially coherent precipitates in a Cu-Mn-Al alloy in different diffracting conditions. Figure 9 shows how such experiments can be used to identify a fault in a more complex material, in this case lithium iron spinel.

In addition to defect characterization more detailed information about faults may be derived with the aid of computer simulation. Application of dynamical electron diffraction theory for interpretation of contrast is well established (Head, Humble, Clareborough, Morton and Forwood, 1973). It is possible then to adjust parameters describing the defect (e.g. lattice distortions near a dislocation) until exact fit is found between the simulated and experimental image. A detailed model may then be found for the configuration of the lattice defect itself. Further refinement is possible due to recent advances in image formation. The image width of a fault is often much greater than the true width (e.g. dislocation images are ~100Å wide whereas we envisage a dislocation core as being only ~3 atomic diameters wide). It can be considerably reduced by imaging not conventionally in strong two beam conditions, but by forming either a dark field image using a weakly diffracted beam (the weak beam method (Cockayne, Ray and Whelan 1969, Cockayne, 1974)) or by taking a bright field micrograph with a high order reflection close to the Bragg condition (Goringe, Hewat, Humphreys and Thomas, 1972). Dislocation images can thus be reduced to about 15Å and a much clearer picture of the defect is revealed (e.g. fig.9f,10). Accordingly, a more satisfactory model of the fault can be used for the simulated image (e.g. Cockayne and Vitek, 1974). It may be noted that this approach for

finding suitable defect models is subject to the limitations imposed by approximations in the appropriate theories. A more satisfactory method is direct imaging of the atomic lattice, as described in section 4.

Most materials can now be thinned sufficiently for transmission of 100kV electrons (either electrolytically (metals), chemically, by cleavage or by ion bombardment (ceramics)). A range of specimen stages is available for in situ studies, as for SEM, and the increasing availability of high voltage instruments (up to 1.5MeV commercially) allows more sophisticated experimentation (Swann, Humphreys and Goringe, 1974). Not only can thicker samples be examined, which is useful for materials difficult to thin and for experiments on foils which are more representative of bulk materials (e.g. Butler and Swann, 1975), but an environmental stage can also be incorporated due to the greater space between the objective lens pole pieces. Thus it is now possible to study solid-gas reactions in the microscope in a controlled atmosphere at high temperature (e.g. Flower and Swann, 1974) and phase transformations in materials which would degrade in the normal vacuum of the microscope (e.g. van der Biest, Butler and Thomas, 1975). Furthermore, the high energy electrons are capable of displacing atoms from their lattice sites so that in situ radiation damage experiments are also possible (Makin, 1971; Laidler and Mastel, 1975).

In summary the current applications of TEM include complete characterization of one, two and three dimensional lattice defects, study of phase transformation processes either in selected samples or in situ in appropriate high temperature stages, phase analysis

of complex materials from electron diffraction patterns, crystallographic analysis of defects and transformation processes, environmental reactions and radiation damage. Much of the desired information concerning the relationship of structure and properties of materials may be gained from TEM.

D. Scanning Transmission Electron Microscopy (STEM)

The scanning transmission electron microscope combines various advantages of the transmission and scanning microscopes (Crewe, Wall and Welter, 1968; Crewe, 1974; Cowley, 1975; Thompson, 1975; Crewe, Langmore and Isaacson, 1975). A thin sample is used (as for TEM), a fine beam is scanned across the specimen (as for SEM) and the transmitted electrons are collected and processed for display on a CRT in synchronization with the scanned incident beam (hence STEM). Under normal circumstances the contrast in the image is identical to that in TEM if a small enough collector angle is used, according to the principle of reciprocity (Cowley, 1969). Thus, it is possible to image defects at high resolution directly in the STEM. Standard electron diffraction patterns may also be obtained by rocking the beam on the specimen and because of the small probe size extremely small areas can be selected for analysis (~30Å diameter compared to ~1μ diameter for TEM (Geiss, 1975a).

Several commercial TEM's have attachments to allow conversion to STEM operation but their resolution is limited to about 30Å by the probe size and thermionic source brightness. By use of a field emission electron source the probe size can be reduced to ~3Å with high intensity. Consequently the resolution achieved can be similar to that of present TEM and with higher accelerating voltages it is predicted

that resolutions lower than 1Å will be attained (Crewe, 1974). One of the first commercial STEM with field emission source has recently been announced (Banbury, Drummond and Ray, 1975) with 3.1Å lattice fringes of silicon readily resolved (fig. 11).

Apart from the microdiffraction capability of STEM there are several other advantages over TEM. Firstly an image can be obtained on the CRT at magnifications up to 20×10^6 times, and relatively rapid exposures taken at this level, compared to typical maximum TEM magnifications of $0.5 - 1 \times 10^6$ times on the final viewing screen. Secondly chromatic aberration does not limit resolution from thick specimen areas as it does in TEM at similar applied voltages (80-120kV) because there are no lenses after the specimen. The inelastically scattered electrons can be separated from the unscattered beams prior to image processing to improve the image contrast. This yields a considerable increase (about five fold) in the specimen thickness that can be examined at high resolution which is comparative to the gain achieved by high voltage TEM (e.g. fig. 12). Thirdly the energy loss spectrum from the specimen is readily available in the STEM and may be obtained with a commercial instrument whereas energy loss analysis in TEM is confined to a few prototype instruments. Fourthly, energy dispersion analysis of characteristic x-rays produced by the electron irradiation (for composition determination) is also readily available on the STEM, as it is for SEM. Fifthly, the gun chamber of a emission STEM must operate at an extremely good vacuum (10^{-11} torr) so that the specimen may also be maintained in good vacuum with a corresponding very low contamination rate.

The advantages of a STEM instrument over a conventional TEM appear to be significant. However, the cost is correspondingly greater and so it seems that defect characterization will continue to be performed on TEM, with STEM remaining a specialist instrument for the next few years. Ultimately, it is predicted that work currently carried out on TEM will be taken over by STEM.

E. X-ray Microscopy* (Topography)

As the wavelength of x-rays is considerably lower ($\lambda \sim 1\text{Å}$) than that for optical light it might be expected that x-ray microscopy (often known as x-ray topography) would also improve the resolution possible for defect studies. However, it is extremely difficult practically to focus x-rays in the same way as light or electrons for the following reasons. Firstly, their refractive index is close to unity for all materials and they are rapidly absorbed. Hence the design of optical-type lenses with low aberrations is not possible. Secondly, being electromagnetic radiation their beam path is unaffected by electrostatic or magnetic lenses. Furthermore, the detection and informational display of x-rays is less efficient than for light or electrons so that instantaneous information about sample areas would not be possible with current technology. X-ray microscopy is therefore confined either to direct one-to-one images which may be enlarged photographically from high resolution photographic film or to magnifications

---

*The information which may be derived indirectly from analysis of diffracted x-ray beams is not considered in this article.

of up to 100 times with various geometrical arrangements. The best resolution possible is about 1μ which is on the same scale as optical microscopy.

The reason that x-ray microscopy is used is that direct micrographs can be taken, at low magnification, of lattice defects in large areas of bulk materials. Optical microscopy relies on indirect methods such as etch pitting for information about finer scale defects such as dislocations. However, the x-ray image is comparable to the electron image, with similar contrast for dislocations, stacking faults, vacancy loops, low angle boundaries, etc. (Young, Baldwin and Sherill, 1967; Authier, 1970; Lang, 1970; Wu and Armstrong, 1975). Dislocations for instance appear as a black line in incident beam images but lack of resolution limits the line width to a minimum of about 2μ (c.f. dislocation image widths as narrow as 15Å may be produced by TEM, see section 3C). It is important to realize that x-ray microscopy does not, and can not, compete with transmission electron microscopy for high resolution detail. Its advantage comes from the ability to produce a picture of the defect distribution in bulk sized specimens, confined to those cases where low defect densities are expected, for example silicon single crystals for semiconductor devices. (An estimate shows that for a dislocation image width of 10μ, individual dislocations will not be resolved if their population density is greater than 10^6 cms^{-2}). Micrographs may be taken in the back-reflection (Berg-Barrett) mode or the transmission (Lang) mode for thin samples (see Lang, 1970; Armstrong and Wu, 1973) and the picture may be recorded photographically or by diffractometer methods. An example showing dislocations in silicon is illustrated in fig. 13. Thus for specialist

applications, most notably examination of crystals for electrical devices, the x-ray microscopy method may be preferred for general examination over optical or electron microscopy, although for detail on a high resolution level the latter would be utilised.

F. Field Ion Microscopy (FIM)

A technique which can resolve individual atoms deserves consideration as a tool for studying lattice defects. The field ion microscope (Muller and Tsong, 1971) forms an image of a highly curved, approximately hemispherical surface of metals and where this surface is parallel to high index planes in the lattice (e.g. {420}, {531}) the individual more widely spaced atoms ($\geq$3Å separation) can be discerned. Image formation occurs by the ionisation of a suitable gas (H, He, Ne, Ar) at positions on the positively charged surface where atoms protrude, generally the outermost atoms on a plane layer (e.g. fig. 14). The newly formed positive gas ions are then attracted away from the specimen to a fluorescent screen at ground potential or more commonly to an image intensification system. The resultant image is approximately a stereographic projection of the surface magnified by the ratio of tip-screen distance to tip radius, typically 10^6-10^7 times. A series of sections can be studied by removal of a controlled amount of material, atom by atom or plane by plane, on raising the tip voltage to the level where the specimen atoms themselves are attracted away (field-evaporation) thus giving a three dimensional view of the sample. In the high index pole regions a column of material (~20-40Å in diameter) may be examined atom by atom.

Contrast can occur on two levels: at the atomic level either by preferential gas ionisation over one atomic species in an alloy (i.e. a brighter image spot (e.g. fig. 15))or by preferential removal of atom species; at a lower level by higher or lower ionisation (hence image brightness (e.g. fig. 16))at the defect or by modification of the crystallographic nature of the image.

The technique is a highly effective one for studying atomic distributions but still remains a specialist research tool which does not appear to be readily available. There is no profitable industry behind FIM and hence instrumental development is slow and confined to prototype instruments and the number of competent users is also correspondingly low. Only a very small statistical sample can be analysed and often it is not possible to gain an adequate perspective of microstructure. The correlation of structure and properties is more readily obtained by TEM, SEM and optical microscopy, and these latter techniques find more wide scale use as they can be employed to solve immediate problems which may arise in the production of components as well as providing a basis for understanding the fundamentals of materials science.

Several further difficulties arise in applying FIM. Although the specimen may be studied atom by atom, the image of the atom positions is distorted from the true lattice positions by the extremely high electrical field. Thus the distortion of the crystal lattice near defects may not be studied. Secondly, most of the area of the image is taken up by the characteristic low index pole rings. Information can easily be lost between these rings (or plane ledges), which are typically ~20Å apart, and thus atomic detail is not achieved in these areas.

Thirdly, the specimen must be able to achieve and sustain a high electrical field at its surface and therefore must be a good electrical conductor. This confines most studies to metals, although not all (e.g. Al, Mg, Zn, Ti) can withstand the high electrostatic forces on the tip during operation. Fourthly, crystallographic information such as orientation relationships may be found after detailed analysis but are often more readily available from techniques involving diffraction.

Nevertheless, if a problem in materials science requires a solution at the atomic level, a well-chosen experiment by FIM is often superior to conventional methods. It is the only tool which can currently image, as a matter of routine, individual point defects in metals. This capability has proved useful in studying the distribution of vacancies and interstitials after radiation damage (O'Connor and Ralph, 1972; Robinson, Wilson and Seidman, 1973) and in determining atomic arrangements in dilute alloys (Gold and Machlin, 1968), in order-disorder systems (Berg, Tsong and Cohen, 1973) and in ordered precipitates (Sinclair, Leake and Ralph, 1974) (e.g. fig. 15). The images of non-dilute alloys (e.g. complex steels) are difficult to interpret due to the disruption of the characteristic ring pattern by the behaviour of the various atomic species both to field evaporation and ionisation.

Some useful high resolution information has been obtained about dislocations by FIM (e.g. Smith, Page and Ralph, 1969; Taunt and Ralph, 1974; Seidman & Burke, 1974) but so few dislocations appear in an image (one every few specimens) that reliable statistics are rare and it is more convenient to scan thin areas in TEM and image in weak beam or high order bright field conditions for high resolution detail (section 3C).

Grain boundary topography may be obtained at a resolution of about 5Å and the technique appears quite promising in this field. Finding a suitable grain boundary is tedious and may be aided by high voltage TEM (Smith,Smith, Taylor, Goringe and Easterling, 1974), but very little of the grain boundary area can be mapped in detail (e.g. ~1000Å x 500Å). The statistical sample may always be questioned when the analysis is extrapolated to explain bulk behaviour (Murr, 1975), but a quite detailed picture of boundaries can be built up. In analysis of three dimensional defects, the method is particularly useful where there is a high defect number density (e.g. fig. 16). FIM can often yield information about homogeneous reactions (e.g. homogeneous nucleation (Driver and Papazian, 1973), spinodal decomposition (Sinclair et al 1974) and ordering (Taunt and Ralph, 1974)) which may be lacking in conventional methods due to lack of resolution or overlapping of fine detail (FIM is a surface technique). Chemical data can also be derived about very small regions by use of an atom probe FIM (Muller, Panitz and MacLane, 1968) in which individual atoms can be identified.

Thus the technique is extremely useful in obtaining atomic detail about radiation damage, grain boundaries and phase transformation processes. Its role would best appear to be complementary to the other techniques to provide specialist detail which is not available from the alternative methods.

G. Methods of Local Chemical Composition Determination.

The localized segregation of the constituents of a material will affect its properties to an extent depending on the scale of the effect and the property under consideration. For instance, segregation or

clustering at the atomic level will affect electrical properties to a larger degree than it would fracture toughness. Conversely grain boundary segregation and precipitation commonly affects toughness but need not be considered for electrical devices made from large single crystals. Thus, chemical investigation on a wide range of scale is desired by the materials scientist. Amongst the various investigative techniques for direct defect observation described above, modifications of the basic approach also allows local chemical composition to be established in known areas and these methods will be described briefly in this section.

(i) Optical Methods

The contrast obtained in polished and etched specimens can often indicate composition differences on a scale within the limit of the optical microscope. It is not possible, however, to establish quantitatively the degree of segregation nor to identify particular phases which may be present without recourse to other techniques. Thus, optical microscopy may be used as an indicator but not when detailed information is required.

(ii) SEM Methods

The large amount of space available near the specimen in the scanning electron mode allows the positioning of detectors suitable for identifying characteristic emitted radiation. The incident electron beam excites electrons in the atoms of the specimen to higher energy states. On subsequent decay to lower energies either characteristic electromagnetic radiation (x-rays) or characteristic (Auger) electrons are emitted. The signals can be processed to determine either quantitatively the amount of various species in the area examined or to yield

a picture of the distribution of a particular species.

The characteristic x-rays may be analysed for wavelength using a crystal spectrometer arrangement or directly for energy using an energy dispersion analyser (Belk, 1974; Philibert and Tixier, 1975). The former has superior characterizing resolution although with recent technological advances in detector systems (e.g. lithium drifted silicon diode detectors) this advantage is less marked and the two are comparative at high x-ray energies (~1Å wavelength) (Gedcke, 1974; Kandiah, 1975). The latter is superior in efficiency of detection and may be preferable for scanning microscopy applications. Elements next to each other in the periodic table can generally be distinguished but the analysis of lighter elements is still difficult. For quantitative analysis it is preferable to obtain, from suitable standard specimens, the variation of characteristic x-ray intensity with material content near the range of interest and for optimum quantitative data purpose-built electron probe microanalysis equipment should be used.

The practical spatial resolution is set by the size of the region from which x-rays are emitted, which depends on the probe diameter, incident electron energy and the constitution of the region from which excita occurs. A sufficiently high intensity x-ray signal must be produced so that in commercial instruments probe diameters are not usually smaller than 1μ. The x-rays also originate from a depth of this order so that volumes ~10^{-12} cms^3 may typically be analysed. The analysis of small particles should be treated cautiously as penetration of the beam through the particle to the underlying matrix may cause errors in the composition determination.

Auger electrons are most efficiently excited by low energy incident electrons (e.g. 1-5 kV) compared with the higher energies favorable for x-ray excitation. The penetration of the electron probe is low and energy loss of the Auger electrons on exit from the sample restricts analysis to surface layers of the specimen (~10Å depth). The spatial resolution is similar to the other electron probe techniques (MacDonald, 1975) and thus the volume analysed is smaller than for x-ray detection. This is advantageous for studying the composition at surfaces e.g. fracture surfaces may be analysed for the presence of deleterious constituents which may be in too low a concentration for detection by other means. A three dimensional analysis can be performed by stripping the original surface by ion sputtering, although eventually this will lead to a rough surface. The efficiency of Auger electron production does not fall off with atomic number as rapidly as x-ray production so that this method is superior for analysing light elements. One disadvantage is the necessity (and expense) of extremely good vacuum at the specimen in order to ensure minimal surface contamination so that the true surface is being examined.

(iii) Transmission Electron Methods

For higher resolution analysis it is necessary to utilise transmission methods. However, the incorporation of detectors for emitted radiation in TEM is considerably more difficult due to lack of space near the specimen and very few TEM instruments take advantage of the characteristic radiations. The commercially available electron microscope with microanalyser (EMMA -4) possesses an optimum resolution of about 0.1μ. Alternatively, it is possible to study the transmitted

electron beam to establish the spectrum of energies due to interaction of electrons with the elements of the crystal through which the beam has passed. The energy loss is dependent upon the species with which interaction has occurred and thus can be used for chemical analysis. The spatial resolution can be reduced to ~100Å by suitable choice of slits to select the transmitted electrons. An example of a comparison of electron velocity analysis with an EMMA analysis of the same specimen area is shown in fig. 17. A disadvantage of electron energy or velocity analysis is that only low atomic number elements have narrow energy loss peaks and are suitable for such analysis (e.g. Al, Mg, Be). Thus superior resolution is gained at the expense of being able to study only a few "model" systems. Also an energy loss analyser for TEM is not widely available and the technique is also confined to a few prototype instruments.

Conversely STEM instruments can readily be designed to include provision for both x-ray and energy loss analysis. Furthermore, the inelastically scattered electrons may be separated from the unscattered beam and utilised in image formation. As the probe size is also considerably smaller than for conventional SEM it seems that improved resolution for analysis will be possible with STEM. The versatility of STEM indicates that it could be an exciting development in the microanalysis field.

(iv) Direct Atom Analysis

Atoms removed from the surface of a specimen may be subsequently analysed by a mass spectrometer for identification. This is the principle of secondary emission analysis whereby ions are removed by bombardment of the

sample with a beam of positive ions (Castaing, 1975). The resultant ion signal may be directly characterized or focussed and a particular element chosen to form an image showing the distribution of this species. The resolution is ~0.5μ, slightly superior to conventional electron probe methods, and in principle it is possible to analyse for any element or isotope.

The atom-probe field-ion microscope is capable of analysing single atoms chosen from a FIM image by timing the flight of the ion between specimen and detector. The composition of extremely tiny regions can be obtained (e.g. Goodman, Brenner and Low (1973)found the composition of Cu-rich G.P. zones during the initial stages of precipitation in an Fe-Cu alloy). As the statistical sample is normally small (~10^3-10^4 atoms analysed) the experiment must be chosen carefully if the results are to be projected as representative of the bulk of the material, but for studies of very fine scale segregation phenomena in metals this is obviously an extremely powerful technique.

4. Lattice and Structure Imaging

Current transmission electron microscopes possess the capability of 2Å line resolution and 3.5Å point-to-point resolution. Thus by suitable choice of imaging conditions it is possible to image directly the crystalline lattice itself. An increasing amount of research has been devoted over the past five years to establishing the conditions under which lattice images can be satisfactorily and readily interpreted in terms of the real lattice of the specimen. The advances which have been made and some applications of the technique will be illustrated in this section.

Two types of image are taken at present: one dimensional lattice fringe images and two-dimensional lattice structure images. In the one dimensional image, electron reflections perpendicular to the desired imaging planes are strongly excited by suitably tilting the specimen and information is derived from only one set of atomic planes in the crystal. This technique provides useful information about metals and other close-packed structures where it is difficult to obtain representative two-dimensional images. The structure image may be taken of more complex materials with larger unit cell dimensions. The interpretable resolution limit is only ~3.5Å point-to-point at present (set by the combination of incident beam divergence and spherical aberration of the objective lens (O'Keefe and Sanders, 1975)) and thus this approach is only appropriate for complex structures.

The experimental variables which affect the lattice image are now well established (Allpress and Sanders, 1973; Lynch, Moodie and O'Keefe, 1975; Sinclair, Schneider and Thomas, 1975). They are:

i) The number of electron beams allowed through the objective aperture to form the image. For satisfactory structure images a minimum number of about 20 reflections is thought necessary for periodic images (Lynch et al, 1975). As the size of the objective aperture, and so number of chosen beams, increases the spherical aberration of the objective lens causes too great a phase shift with respect to the transmitted beam and eventually loss of resolution is encountered. An objective aperture of 40-50μ diameter is typically employed. Many beams from all directions in the crystal are used in image formation, with the diffraction pattern normally set close to a low index zone orientation. At appropriate microscope

settings the image represents a projection of the electron density in the specimen and may be interpreted accordingly (Cowley and Iijima, 1972; O'Keefe, 1973). In fringe images only two or three beams are utilized, although for metals it is interesting that this requires a similar aperture size to that used for complex structure imaging.

ii) The orientation of the specimen. As outlined above, a systematic row of reflections is used for lattice images whereas a complete zone is utilized in structure imaging. It is important to be very close to an exact Bragg reflecting condition for the former (Hirsch et al, 1965; Sinclair et al, 1975) and to the exact zone axis in the latter case (Iijima, 1971, 1973; Cowley and Iijima, 1972).

iii) The objective lens setting. The lattice image is essentially a phase contrast image formed by interaction of electron waves with various amplitudes and phases. Because of the spherical aberration of the objective lens electron beams off the optical axis of the microscope suffer a phase delay with respect to the central beam which may be counteracted by defocus of the objective lens from the true Gaussian focus plane. The amount of defocus (optimum defocus condition (Scherzer, 1949))depends for each microscope on the spherical aberration coefficient. For the JEM 100B used by Iijima the optimum defocus is 900Å (Cowley and Iijima, 1972). For the Philips EM301 used by the present author for superlattice imaging in Cu_3Au the value is 300Å underfocus (Sinclair et al, 1975). The exact setting must be found for each case by appropriate calculations or in practice by choosing the most suitable image from a through-focus series of micrographs.

iv) Specimen thickness. By increasing the thickness of a TEM specimen the intensity of transmitted and diffracted electron beams is affected. Thus certain thicknesses are optimum for suitable images and these may be found by the appropriate calculations or by inspection of the image of wedge-shaped specimens. For structure images foils $\lesssim$100Å thick are preferred although an identical image may be obtained at much greater thicknesses (e.g. in H-Nb_2O_5 the image at 500-800Å thickness is identical to that in the thin sub-100Å area (Fejes, Iijima and Cowley, 1973). For two beam fringe images, the optimum thicknesses occur at $\xi g/4$, $3\xi g/4$, $5\xi g/4$, etc. (ξg = extinction distance of the reflection) with the first being the best (Phillips, 1971). It is desirable therefore to have thin, high quality foils for lattice imaging, which may be prepared from bulk in the normal way (see section 3C) or, for metals, prepared to the optimum thickness by vapour deposition techniques (Sinclair et al, 1975).

Various other considerations are also important. The mechanical, electrical and thermal stability of the microscope must be extremely good to allow 2Å resolution, especially since exposure times up to 60 seconds may be required. Specimen drift (e.g. due to heating or charging in the intense electron beam) must be minimised and the material should not degrade in the beam (this is a serious problem in imaging organic materials at high resolution). The contamination rate should be low. The objective aperture should be positioned carefully to reduce any effect it may have on the electron beams and it should preferably be of the thin film type which suffers low contamination. It is also extremely important to correct the astigmatism of the objective

lens as carefully as possible. This should be done on the area under examination and should be recorrected after any changes of specimen position, orientation or even objective aperture location.

Finally, it should be emphasized that the interpretation of the images and the determination of optimum experimental conditions is best approached by theoretical image simulation. For structure images, phase grating multi-slice calculations are preferred whereas for the simpler fringe images the Bloch wave method of dynamical electron diffraction theory may be utilized. In this way ambiguous or incorrect interpretation may be avoided.

A. Ceramics

Fringe imaging was applied to examine defects in ceramics before the higher resolution structure imaging was attempted (e.g. Allpress and Sanders, 1972). Information was obtained about planar defects in the Nb_2O_5-WO_3 and Nb_2O_5-TiO_2 systems which are present to accommodate non-stoichiometry from crystallographically simpler structures. Elsewhere fringe images have been used in studies of phase transformations in orthopyroxene (Vander Sande and Kohlstedt, 1974; Champness and Lorimer, 1974) and defects in hexagonal ferrites (Van Landuyt, Amelinckx, Kohn and Eckart, 1973, 1974). However, the most important work on ceramics has come from structure imaging.

At the appropriate underfocus the structure image can be interpreted in terms of a projection of the charge density of the material (Cowley

and Iijima, 1972). Thus in metallic oxides the projection of metal atom rows appears dark on the image whilst rows of oxygen atoms appear light. Metal atoms too close to one another for resolution appear as darker regions than those which can be resolved by the microscope. The image is essentially a charge density map of the structure. An example of this correlation between the electron structure image of $Ti_2Nb_{10}O_{29}$ and the projection of the structure as established by x-ray diffraction is shown in fig. 18a,b and that for a silicate (beryl) in fig. 18d. Other materials so imaged include various Ti, Nb and W oxides (Iijima and Allpress, 1973, 1974), silicates (Buseck and Iijima, 1974), wüstite (Iijima, 1974), perovskite polytypes (Hutchison and Jacobson, 1975), and tournaline (Iijima, Cowley and Donnay, 1973). The correlation between the structure and projected images indicates that structure determination itself is possible if a reasonable basis of the structure is known. Examples whereby ambiguities of x-ray structures were resolved in various tetragonal tungsten bronze type materials in the Nb_2O_5-WO_3 system have been described by Iijima and Allpress (1973, 1974).

The advantage of using a direct technique such as microscopy to view defects is that their nature and distribution can be observed directly on a picture. The further advantage of structure and fringe imaging is that the atomic arrangement at the defect can be seen. An example of the effect of a planar defect on the atomic arrangement in H-Nb_2O_5 (Iijima, 1973) is shown in fig. 19. The change of stacking sequence is quite clear and a shift of the fault plane is also revealed at the atomic level. Point defects in $Nb_{12}O_{29}$ and $Nb_{22}O_{54}$ (Iijima, Kimura and Goto, 1973, 1974) are shown in fig. 20a,c. A model for the

defect based on local changes of metal atom positioning is shown in fig. 20d for the latter. It is interesting that after a few minutes irradiation under the electron beam these defects can be made to disappear (fig. 20b), although in some cases they reappear in different parts of the image (Iijima et al, 1974). This indicates that the dark spots are very likely to be point defects which can be induced to diffuse by beam heating or irradiation. Thus the structure imaging technique is capable of imaging even point defects in materials and gives much unequivocal data on the character of defects in ceramics.

B. Metals

In metallurgy, in which the crystal structures are simpler, much of the interest has centered around application of the method to defect and phase transformation studies. Considerable excitement was aroused at the first direct lattice fringe image of a dislocation whereby a terminating atom plane was surrounded by planes distorted from their natural position (e.g. fig. 21a, from Phillips and Hugo, 1970). It was supposed that plane distortions could be measured directly from the image. However, Cockayne, Parsons and Hoelke (1971) showed that, since very few dislocations lie parallel to the imaging planes, the inclination of the dislocation line will contribute strongly to the observed fringe positions. From simulated images it was learned that there is not in general a one-to-one correspondence between fringe and atom plane positions in such circumstances. It can be seen for instance in fig. 21 that the fringe distortions are not symmetrical with respect to the terminating fringe, with greater disruption of the image on the right, whereas the atomic plane distortions should be symmetrical about an

isolated dislocation. Thus one must be extremely cautious in choosing faults for analysis by lattice imaging. Care must also be taken over other electron optical effects, such as fringe bending at the edge of thin foils, the causes of which are outlined by Hirsch et al (1965). Nevertheless, it is becoming clear that, as in structure images, if the fault lies parallel to the imaging planes then fringe images may be associated with atomic plane positions (for a dislocation this may be ensured by a perfectly symmetrical lattice fringe pattern about the terminating fringe (Cockayne, 1975)) as in Fig. 21b, and that lattice imaging may be utilized for studying defects in appropriate circumstances.

The superior information available from lattice imaging of alloys over conventional imaging modes is illustrated by fig. 22 which compares the lattice image and superlattice dark field image of an antiphase boundary (APB) in ordered Ni_4Mo. In the latter the boundary is revealed as a black line on a white background, in some regions ~20Å thick. The translation at the APB must be determined by series of various dark field micrographs. However, the lattice image can be taken as representing the positions of the Mo plane of atoms, which occur every fifth plane in the superlattice with the other planes being all Ni. The continuity of the fringes (atomic planes) is shown to within an atomic diameter of the fault. From calculations of the fringe visibility with degree of long range order it is established that little change in degree of order occurs up to the APB. It can be seen directly that the left-hand side is shifted upwards by the two-fifths of the superlattice spacing (i.e. two fundamental lattice planes) with respect to the right and that there is a local change of spacing (and hence

composition) where the boundary becomes parallel to the imaging planes (arrowed). Considerably more information is present in the lattice image which is not available from the conventional micrograph.

A lattice image of fully ordered Mg_3Cd is shown in fig. 23, in which the domain structure and several faults are clearly revealed. The orientation of each domain is shown directly and the very flat crystallographic nature of the domain interfaces is illustrated. A further comparison of the lattice and dark field image is shown in fig. 24 for partially ordered Mg_3Cd. The bright areas in the superlattice dark field image represent ordered regions, the dark regions are disordered. In the lattice image this is revealed by differences in fringe spacings with double periodicity in the ordered material (Rocher, Dutkiewicz and Thomas, 1975; Sinclair and Dutkiewicz, 1975). In some regions ribbons of ordered material are present in which the interface shows a slight bending. The lattice image reveals why this occurs (fig. 25). There are discrete unit cell high steps at the interface which are not revealed in the dark field image. This suggests that the mechanism of ordering in this alloy is one of movement of these steps across the interface and this would also account for the flat domain boundaries found in the fully ordered alloy (fig. 23). Again it can be appreciated that superior information is available in the lattice image.

To date, the technique has been used to study dislocations and twins in various metals and semiconductors (Phillips, 1971) radiation damage in copper (Howe and Rainville, 1972) precipitation and single atom layer G.P. zone formation in Al-Cu (Parsons, Rainville and Hoelke, 1970; Phillips, 1973, 1975) and Cu-Be (Phillips and Tanner, 1973). The

interest of our group has been in studying short-range order (Sinclair and Thomas, 1975) ordering reactions and defects in ordered alloys (Sinclair et al 1975; Sinclair and Dutkiewicz, 1975; Dutkiewicz and Thomas, 1975) and spinodal decomposition processes (Gronsky, Okada, Sinclair and Thomas, 1975). As in studies of ceramics the technique is superior to conventional imaging for yielding information at the atomic level.

C. Amorphous Materials.

Interpretation of the structural nature of amorphous materials has been ambiguous since it was found that the diffraction pattern showed diffuse peaks at well-defined angular positions. Renewed interest in this problem has come from lattice imaging of such materials. Rudee and Howie (1972) formed images using the transmitted beam plus part of the first diffuse ring and found regions ~14Å in diameter in amorphous Si and Ge films possessing regular fringes. These they interpreted as small crystallites existing in the predominantly irregular structure. However, more recent experiments (Herd and Chaudhari, 1974) on a range of amorphous films has indicated that their result was an imaging artifact arising from lens astigmatism on tilting the electron illumination and that the extent of coherently scattering regions is $\lesssim$6Å. It was concluded that the random network model is more appropriate for describing amorphous structures. This latter conclusion has also been drawn from independent microdiffraction experiments on specimen areas ~30Å in diameter using a STEM (Geiss, 1975b). It may be noted that these experiments illustrate the care that must be taken over interpretation of lattice images.

5. Summary and Conclusions

A wide range of investigative methods are available for studying and characterising defects in materials. These range from direct visual observation down to the resolution of individual atoms by transmission electron microscopy or field-ion microscopy. Most structure characterization laboratories are equipped with optical, SEM and TEM facilities and these offer the capability of studying each of the various crystal defects (c.f. fig. 1). These techniques should be regarded as complementary rather than directly competitive and the approach taken by the investigator should be carefully considered according to the problem to be solved.

For future trends it seems that direct lattice imaging by TEM will prove extremely useful for obtaining information about fine-scale detail of defects which is not currently available. Further direct, conventional information about microstructure and defect characteristics is also available at lower resolutuion in the same instrument. The scanning transmission electron microscope also appears a considerably more versatile instrument than the conventional transmission microscope and if the cost becomes competitive much basic research may well be transferred to this mode. In any event the materials scientist has a wide scope in characterising the defects which affect the properties of materials.

Acknowledgements

Financial support for this work has been provided by the National Science Foundation and the Energy Research and Development Agency. The author would like to acknowledge the encouragement given by Professor G. Thomas during preparation of this article and, for helpful and critical discussion, Dr. D. R. Clarke and the other members of the electron microscopy group in the Materials Science Department at Berkeley. Thanks are also due to the authors, cited in the figure captions, who kindly provided micrographs for illustration.

REFERENCES

J. G. Allpress and J. V. Sanders (1972) Electron Microscopy and Structure of Materials, edited by G. Thomas et al, Univ. of Calif. Press (Berkeley) p. 134.

J. G. Allpress and J. V. Sanders (1973) Jnl. Appl. Cryst. 6, 165.

S. Amelinckx, R. Gevers, G. Remaut and J. Van Landuyt (1970) Modern Diffraction and Imaging Techniques in Material Science, North Holland (Amsterdam).

R. W. Armstrong & C. C. Wu (1973) Microstructural Analysis: Tools & Techniques, edited by J. L. McCall and W. M. Mueller, Plenum (New York) p. 169.

A. Authier (1970) Modern Diffraction and Imaging Techniques in Material Science, edited by S. Amelinckx, et al., North Holland (Amsterdam) p.481.

J. R. Banbury, I. W. Drummond and I. L. F. Ray (1975) Proc. 33rd Ann. Conf. EMSA p. 112.

J. A. Belk (1974) Quantitative Scanning Electron Microscopy, edited by D. B. Holt, et al. Academic Press (London) p. 389.

H. Berg, T. T. Tsong and J. B. Cohen (1973) Acta. Met. 21, 1589.

G. R. Booker (1970), Scanning Electron Microscopy, Proc. 3rd Annual SEM Symposium, Chicago, IIT Research Institute (Chicago) p. 489.

M. Bouchard, R. J. Livak and G. Thomas (1972) Surf. Sci. 31, 275.

A. N. Broers (1969) Rev. Sci. Instr. 40, 1040.

L. M. Brown (1971) Electron Microscopy in Material Science, edited by U. Valdré, Academic Press (New York) p. 360.

P. R. Buseck and S. Iijima (1974) Am. Min. 59, 1.

E. P. Butler and P. R. Swann (1975) Physical Aspects of Electron Microscopy and Microbeam Analysis, edited by B. M. Siegel and D. R.

Beaman, Wiley (New York) p. 129.

R. Castaing (1975), Physical Aspects of Electron Microscopy and Microbeam Analysis, edited by B. M. Siegel and D. R. Beaman, Wiley (New York) p. 355.

P. E. Champness and G. W. Lorimer (1974) Phil. Mag. 30, 357.

D. R. Clarke (1971) Phil. Mag. 24, 973.

D. J. H. Cockayne (1974) Jnl. de Phys. 35, C7-12.

D. J. H. Cockayne (1975) Proc. 33rd Ann. Conf. EMSA (Las Vegas) p. 2.

D. J. H. Cockayne, I. L. F. Ray and M. J. Whelan (1969), Phil. Mag. 20, 1265.

D. J. H. Cockayne, J. R. Parsons and C. W. Hoelke (1971), Phil. Mag. 24, 139.

D. J. H. Cockayne and V. Vitek (1974) Phys. Stat. Sol. (b) 65, 751.

J. M. Cowley (1969), Appl. Phys. Lett. 15, 58.

J. M. Cowley (1975), Physical Aspects of Electron Microscopy and Microbeam Analysis, edited by B. M. Siegel and D. R. Beaman, Wiley (New York) p. 17.

J. M. Cowley and S. Iijima (1972) Z. Naturforsch. 27a, 445.

A. V. Crewe (1974) Quantitative Scanning Electron Microscopy, edited by D. B. Holt, et al. Academic Press (London) p. 65.

A. V. Crewe, J. Wall and L. M. Welter (1968) Rev. Sci. Instr. 40, 241.

A. V. Crewe, J. P. Langmore and M. S. Isaacson (1975) Physical Aspects of Electron Microscopy and Microbeam Analysis, edited by B. M. Siegel and D. R. Beaman, Wiley (New York) p. 47.

D. J. Dingley and J. W. Steeds (1974) Quantitative Scanning Electron Microscopy, edited by D. B. Holt, et al. Academic Press (London) p. 487.

P. Doig, J. W. Edington and M. H. Jacobs (1975) Phil. Mag. 31, 285.

J. H. Driver and J. M. Papazian (1973) Acta Met., 21, 1139.

J. Dutkiewicz and G. Thomas (1975) Met. Trans. 6A (in press).

P. L. Fejes, S. Iijima and J. M. Cowley (1973) Acta Cryst. A29, 70.

H. M. Flower and P. R. Swann (1974) Acta Met., 22, 1339.

D. A. Gedcke (1974) Quantitative Scanning Electron Microscopy, edited by D. B. Holt, et al. Academic Press (London) p. 403.

R. H. Geiss (1975a) Appl. Phys. Lett. 27, 174.

R. H. Geiss (1975b) Proc. 33rd Ann. Conf. EMSA (Las Vegas) p. 218.

A. M. Glauert (1972) Practical Methods in Electron Microscopy, 1 North Holland (Amsterdam);

(1974) ibid 2.

E. Gold and E. S. Machlin (1968) Phil. Mag. 18, 453.

S. R. Goodman, S. S. Brenner and J. R.Low (1973) Met. Trans. 4, 2371.

M. J. Goringe, E. A. Hewat, C. J. Humphreys and G. Thomas (1972) Proc. 5th Eur. Cong. on El. Micr., p. 538.

R. Gronsky (1974) M.S. Thesis, University of California, Berkeley.

R. Gronsky, M. Okada, R. Sinclair and G. Thomas (1975) Proc. 33rd Ann. Conf. EMSA (Las Vegas) p. 22.

R. Gronsky and G. Thomas (1975) Acta Met. (in press).

A. K. Head, P. Humble, L. M. Clareborough, A. J. Morten and C. T. Forwood (1973) Computed Electron Micrographs and Defect Identification, North Holland (Amsterdam)

J. W. S. Hearle (1972) The Use of the Scanning Electron Microscope, edited by J. W. S. Hearle, et al., Pergamon (Oxford) p. 1.

J. W. S. Hearle, J. T. Sparrow and P. M. Cross (1972) The Use of the Scanning Electron Microscope, Pergamon Press (Oxford)

S. R. Herd and P. Chaudhari (1974) Phys. Stat. Sol. (a) 26, 627.

P. B. Hirsch, A. Howie, R. B. Nicholson, D. W. Pashley and M. J. Whelan (1965) Electron Microscopy of Thin Crystals, Butterworths (London)

D. B. Holt (1974) Quantitative Scanning Electron Microscopy, edited by D. B. Holt, et al. Academic Press (London) p. 335.

D. B. Holt, M. D. Muir, P. R. Grant and I. M. Boswarva (1974) Quantitative Scanning Electron Microscopy, Academic Press (London).

L. M. Howe and M. Rainville (1972) Rad. Eff., 16, 203.

J. L. Hutchison and A. J. Jacobson (1975) Acta Cryst. B31, 1442.

S. Iijima (1971) Jnl. App. Phys. 42, 5891.

S. Iijima (1973) Acta Cryst. A29, 18.

S. Iijima (1974) Proc. 32nd Ann. Conf. EMSA (St. Louis) p. 352.

S. Iijima and J. G. Allpress (1973) Jnl. Sol. St. Chem. 7, 94.

S. Iijima and J. G. Allpress (1974) Acta Cryst. A30, 22.

S. Iijima, J. M. Cowley and G. Donnay (1973) Tschermaks Min. Petr. Mitt. 20, 216.

S. Iijima, S. Kimura and M. Goto (1973) Acta Cryst. A29, 632. (1974) ibid A30, 251.

O. Johari (1968-1975) Scanning Electron Microscopy. Proceedings of 1st-8th Annual SEM Symposium, Chicago, IIT Research Institute (Chicago).

V. E. Johnson (1975) Scanning Electron Microscopy. Proceedings 8th Annual SEM Symposium, Chicago, IIT Research Institute (Chicago) p. 763.

D. C. Joy (1974) Quantitative Scanning Electron Microscopy, edited by D. B. Holt, et al. Academic Press (London) p. 131.

D. C. Joy, M. N. Thompson, G. R. Booker and W. H. J. Andersen (1974) Phys. Stat. Sol. (a) 21, K1.

K. Kandiah (1975) Physical Aspects of Electron Microscopy and Microbeam Analysis, edited by B. M. Siegel and D. R. Beaman, Wiley (New York) p. 395.

J. J. Laidler and B. Mastel (1975) Physical Aspects of Electron Microscopy and Microbeam Analysis, edited by B. M. Siegel and D. R. Beaman, Wiley (New York) p. 103.

A. R. Lang (1970) Modern Diffraction & Imaging Techniques in Material Science, edited by S. Amelinckx et al. North Holland (Amsterdam) p. 407.

E. Lifshin, W. G. Morris and R. B. Bolon (1969) J. Metals, 21, 1.

D. F. Lynch, A. F. Moodie and M. A. O'Keefe (1975) Acta Cryst. A31, 300.

N. C. MacDonald (1975) Physical Aspects of Electron Microscopy and Microbeam Analysis, edited by B. M. Siegel and D. R. Beaman, Wiley (New York) p. 431.

M. J. Makin (1971) Jernkonterets Ann. 155, 509.

R. K. Mishra (1975) Ph.D. Thesis, University of California, Berkeley. (in progress).

M. D. Muir (1974) Quantitative Scanning Electron Microscopy, edited by D. B. Holt, et al. Academic Press (London) p. 3.

E. W. Muller, J. Panitz and S. B. McLane (1968) Rev. Sci. Instr. 39, 83.

E. W. Muller and T. T. Tsong (1971) Field-ion Microscopy - Principles and Applications, Elsevier (New York).

L. E. Murr (1975) Physical Aspects of Electron Microscopy and Microbeam

Analysis, edited by B. M. Siegel and D. R. Beaman, Wiley (New York) p. 163.

B. V. Narasimha Rao (1975) M.S. Thesis, University of California, Berkeley.

B. V. Narasimha Rao and G. Thomas (1975) Mat. Sci. & Eng. 20, 195.

C. W. Oatley (1972) The Scanning Electron Microscope, Cambridge University Press (Cambridge).

G. P. O'Connor and B. Ralph (1972) Phil. Mag. 26, 113; 129.

M. A. O'Keefe (1973) Acta Cryst. A29, 389.

M. A. O'Keefe and J. V. Sanders (1975) Acta Cryst. A31, 307.

J. R. Parsons, M. Rainville and C. W. Hoelke (1970) Phil. Mag. 21, 1105.

J. Philibert and R. Tixier (1975) Physical Aspects of Electron Microscopy and Microbeam Analysis, edited by B. M. Siegel and D. R. Beaman, Wiley (New York) p. 333.

V. A. Phillips (1967) Techniques in Metals Research, edited by R. F. Bunsah, Wiley (New York) 1, p. 25.

V. A. Phillips (1971) Modern Metallographic Techniques and Their Application, Wiley (New York).

V. A. Phillips (1973) Acta Met. 21, 219.

V. A. Phillips (1975) Acta Met. 23, 751.

V. A. Phillips and J. A. Hugo (1970) Acta Met. 18, 123.

V. A. Phillips and L. E. Tanner (1973) Acta Met. 21, 441.

V. A. Phillips and R. Wagner (1973), J. Appl. Phys., 44, 4252.

J. T. Robinson, K. L. Wilson and D. N. Seidman (1973) Phil. Mag. 27, 1417.

A. Rocher, J. Dutkiewicz and G. Thomas (1975) to be published (University of California, LBL 3559).

M. L. Rudee and A. Howie (1972) Phil. Mag. 25, 1001.

O. Scherzer (1949) Jnl. Appl. Phys. 20, 20.

D. N. Seidman and J. J. Burke (1974) Acta Met. 22, 1301.

K. Seshan (1975) Ph.D. Thesis, University of California, Berkeley.

K. Seshan and J. Washburn (1972) Jnl. Rad. Eff. 14, 267.

B. M. Siegel and D. R. Beaman (1975) Physical Aspects of Electron Microscopy and Microbeam Analysis, Wiley (New York).

R. Sinclair, B. Ralph and J. A. Leake (1973) Phil. Mag. 28, 1111.

R. Sinclair, J. A. Leake and B. Ralph (1974) Phys. Stat. Sol. (a) 26, 285.

R. Sinclair and J. Dutkiewicz (1975) Proc. 33rd Ann. Conf. EMSA (Las Vegas) p. 10.

R. Sinclair and G. Thomas (1975) Jnl. Appl. Cryst. 8, 206.

R. Sinclair, K. Schneider and G. Thomas (1975) Acta Met. 23, 873.

D. A. Smith, T. F. Page and B. Ralph (1969) Phil. Mag. 19, 231.

G. D. W. Smith, D. A. Smith, G. S. Taylor, M. J. Goringe and K. Easterling (1974) High Voltage Electron Microscopy, edited by P. R. Swann et al. Academic Press (London) p. 240.

R. M. Stern, T. Ichinokawa, S. Takashima, H. Hashimoto and S. Kimoto (1972) Phil. Mag. 26, 1495.

P. R. Swann, C. J. Humphreys and M. J. Goringe (1974) High Voltage Electron Microscopy, Academic Press (London).

R. J. Taunt and B. Ralph (1974) Phil. Mag. 30, 1379.

R. J. Taunt and B. Ralph (1974) Phys. Stat. Sol. (a) 24, 207.

G. Thomas (1973) The Science of Materials Used in Advanced Technology, edited by E. R. Parker and U. Colombo, Wiley (New York) p. 35.

G. Thomas, R. M. Fulrath and R. M. Fisher (1972) Electron Microscopy and Structure of Materials, University of California Press, Berkeley.

M. G. R. Thompson (1975) Physical Aspects of Electron Microscopy and Microbeam Analysis, edited by B. M. Siegel and D. R. Beaman, Wiley (New York) p. 29.

P. R. Thornton (1968) Scanning Electron Microscopy, Chapman & Hall (London).

O. O. van der Biest, E. P. Butler and G. Thomas (1975) Proc. 33rd Annual Conf. EMSA (Las Vegas) p. 36.

O. O. van der Biest and G. Thomas (1974) Phys. Stat. Sol.(a) 24, 65.

J. B. Vander Sande and D. L. Kohlstedt (1974) Phil. Mag. 29, 1041.

J. Van Landuyt, S. Amelinckx, J. A. Kohn and D. W. Eckart (1973) Mat. Res. Bull. 8, 1173.

(1974) Jnl. Sol. St. Chem. 9, 103.

L. H. Veneklasen (1975) Physical Aspects of Electron Microscopy and Microbeam Analysis, edited by B. M. Siegel and D. R. Beaman, Wiley (New York) p. 315.

C. C. Wu and R. W. Armstrong (1975) Phys, Stat. Sol.(a)29, 259.

H. Yakowitz (1974) Quantitive Scanning Electron Microscopy, edited by D. B. Holt, et al. Academic Press (London) p. 451.

F. W. Young, T. O. Baldwin and F. A. Shirill (1967) Lattice Defects and their Interaction, edited by R. R. Hisiguti, Gordon & Breach (New York).

Figure Captions

Figure 1. A schematic diagram showing the scale over which the various lattice defects extend and the useful range of the investigative techniques.

Figure 2. A schematic representation of the origin of some contrast effects in optical microscopy of polished and etched specimens.

Figure 3. Optical micrograph of 69.3%Cu 19.4%Ni 11.3%Fe aged for 150 hrs. at 840°C showing the effect on the microstructure of enhanced precipitate coarsening at grain boundaries (courtesy of R. Gronsky, 1974).

Figure 4. A schematic representation of the area near the specimen in the scanning electron microscope.

Figure 5. Scanning electron micrograph (secondary emission mode) of a fractured carbon fibre-epoxy composite. The protrusion of 8μ diameter fibres from the epoxy matrix is vividly revealed owing to the large depth of field of the SEM. Small holes which weaken the fibres can be seen in several cases. (courtesy of D. R. Clarke, 1975, private communication).

Figure 6. SEM fractographs (secondary emission mode) of Fe 4%Cr 0.4%C martensitic steels. (a) Conventionally heat treated material with large prior austenitic grain size (~300μ) suffers quench-cracking and fails by an intergranular mechanism, as clearly shown by the fractograph. (b) The fracture toughness may be increased by nonconventional heat-treatments which give rise to a material which undergoes ductile transgranular failure with a dimple-like fracture surface.

(courtesy of B.V. Narasimha Rao, 1975; B.V. Narasimha Rao and G. Thomas, 1975)).

Figure 7. Schematic representation of the imaging modes in transmission electron microscopy: (a) bright field imaging, (b) dark field imaging with tilted illumination, (c) lattice imaging with tilted illumination.

Figure 8. Bright field electron micrographs (a-c) and corresponding selected area electron diffraction pattern (d) of $Cu_{2.5}Mn_{0.5}Al$ aged for 10^4 minutes at 300°C. The network of lines represents dislocations at the precipitate-matrix interface in the alloy. With the operating reflection g = (200), (020) (b,c) one set of dislocations is revealed, whereas both sets appear in the image when g = (220). These and similar contrast experiments show that the Burger's vectors of the dislocations are of the type $\frac{a}{2}\langle 100\rangle$. (Courtesy of M. Bouchard, R.J. Livak and G. Thomas, 1972).

Figure 9. A series of high voltage (650kV) transmission electron microscopy contrast experiments is shown to establish the nature of a stacking fault in lithium iron spinel. The fault (described by a displacement vector $\underline{R}$) gives rise to a phase change of $\pm\pi$ in the electron waves as evidenced by the symmetry of the stacking fault fringes. It goes out of contrast (c,e,f) when $\underline{g}.\underline{R}$ = zero or integer, whereas the bounding partial dislocations disappear when $\underline{g}.\underline{b} = 0$ (e). The fault vector is thus found to be $\underline{R} = \pm\frac{1}{4}[0\bar{1}1]$, the Burger's vectors of the partial dislocations have $\underline{b} = \frac{1}{4}[0\bar{1}1]$ and the

fault plane is $(0\bar{1}1)$. The images, however, cannot distinguish between extrinsic and intrinsic π-faults in this material (i.e. whether material has locally been "inserted" or "removed" from the structure) and direct lattice imaging would be necessary to establish this aspect of the fault. In addition, by comparing (c) and (f) it can be seen that the dislocation image widths are decreased by imaging in high order bright field conditions (f). (courtesy of R. K. Mishra, 1975; for method, see van der Biest and Thomas, 1974).

Figure 10. A comparison of the conventional bright field image (a) and the weak beam dark field image (b) of ion-implantation damage in silicon. The morphology of the radiation damage is much clearer in the weak beam image (courtesy of K. Seshan, 1975; Seshan and Washburn, 1972).

Figure 11. Lattice image of the (111) planes in silicon as resolved by a commercial scanning transmission electron microscope (courtesy of I.L.F. Ray, 1975, private communication; see also Banbury et al, 1975).

Figure 12. Scanning transmission electron micrograph of dislocations imaged in a thick area of a silicon specimen. (courtesy of I.L.F. Ray, 1975, private communication).

Figure 13. X-ray micrograph of dislocations in a silicon single crystal (courtesy of E. Meieran, 1975, private communication).

Figure 14. Schematic diagram showing the origin of the characteristic ring pattern in field-ion micrographs of metals. The curved section is an isopotential contour and atoms close to this section are imaged.

Figure 15. A field-evaporation sequence showing the stripping, a few atoms at a time, of a (420) plane in a partially ordered γ' precipitate in Ni 14%Ti, aged for 4 hours at 600°C. Alternate rows of atoms are Ni and Ti, the latter appearing brighter and being more susceptible to field evaporation. A nickel atom misplaced in a titanium atom site is indicated in (d). (See Sinclair et al, 1973).

Figure 16. Field-ion micrograph (a) and corresponding stereographic map (b) of Ni 14%Ti aged to peak hardness (500 hours at 600°C). The bright regions are γ' precipitates which are revealed in a characteristic distribution, aligned periodically in <100> directions. (See Sinclair et al, 1974).

Figure 17. A comparison of the determination of the Cu distribution near a grain boundary in an aged Al-Cu alloy by electron velocity analysis (a) and electron microscopy with microanalysis, EMMA (b). (courtesy of D. Doig, J. W. Edington and M. H. Jacobs, 1975).

Figure 18. A comparison of the structure image (a) of $Ti_2Nb_{10}O_{29}$ with a projection of the structure (b). The unit cell indicated in the latter has dimensions $\underline{a}$ = 28.5Å, $\underline{c}$ = 20.5Å and is composed of two layers (dark and light lines) of metal atoms

in oxygen tetrahedra (shaded squares). The corresponding electron diffraction pattern is shown in (c) with a circle indicating the size of the objective aperture. (courtesy of J. M. Cowley and S. Iijima, 1972).

(d) A similar comparison for the structure image of beryl. (courtesy of P. R. Buseck and S. Iijima, 1974).

Figure 19. (a) Structure image of H-Nb_2O_5 showing displacement defects. The unusual black dots in the overlapping region of two defects (in the rectangular box) can be explained by a superposition of the two different arrangements of structural blocks shown in (b) and (c). (courtesy of S. Iijima, 1973).

Figure 20. Structure images showing point defects in $Nb_{12}O_{29}$ (a) and $Nb_{22}O_{54}$ (c). After a few minutes electron beam irradiation of the former, the black dots representing the defects can be seen to have disappeared (b). A proposed model for the origin of the black dots in $Nb_{22}O_{54}$ is shown in (d). (courtesy of S. Iijima, S. Kimura and M. Goto, 1974).

Figure 21. (a) A lattice fringe image of a dislocation in germanium. A terminating fringe is clearly shown but the asymmetric distortion of fringes indicates that the dislocation line is not parallel to the imaging planes and that fringe positions may not be interpreted as representing directly the lattice plane positions (courtesy of V.A. Phillips and J.A. Hugo, 1970).

(b) Lattice image of an edge dislocation in germanium, with symmetrical fringe distortion about the terminating fringe indicating that the dislocation line is parallel to the imaging planes. The fringe distortions in this case should represent lattice plane distortions in the crystal (courtesy of Phillips and Wagner, 1973).

Figure 22. A comparison of the lattice image (a) and conventional superlattice dark field image (b) of an antiphase boundary in ordered Ni_4Mo. Information in the lattice image is given concerning the positions of atomic planes right up to the boundary, the degree of order in the vicinity of the boundary, the nature of the fault and any local composition changes (as in the position indicated). Such detailed information is not available in the dark field image.

Figure 23. A lattice image showing the distribution of domains in ordered Mg_3Cd. It can be seen that rotational domain boundaries and translational antiphase boundaries (as at a) are smooth at an atomic level in this alloy. (courtesy of J. Dutkiewicz, 1975, private communication).

Figure 24. A comparison of the lattice image (a) and superlattice dark field image (b) of partially ordered Mg_3Cd. Ordered regions possess twice the fringe periodicity of disordered regions in the lattice image. An exact correspondence between the two is clear, with more detailed information present in the former (see fig. 25). The corresponding

diffraction pattern is shown in (c) with the smaller circle showing the objective aperture used for the dark field image (b) and the larger circle that the for lattice image (a). (courtesy of J. Dutkiewicz, 1975, private communication).

Figure 25. A detail of the lattice (a) and dark field (b) images shown in fig. 24. The dark field image reveals thin ribbons of ordered material which show some curvature. The lattice image indicates that this is due to unit cell high steps in the interface between ordered and disordered material. In addition to the higher resolution, information about local degree of order can also be obtained from the lattice image but not from the dark field image. (courtesy of J. Dutkiewicz, 1975, private communication).

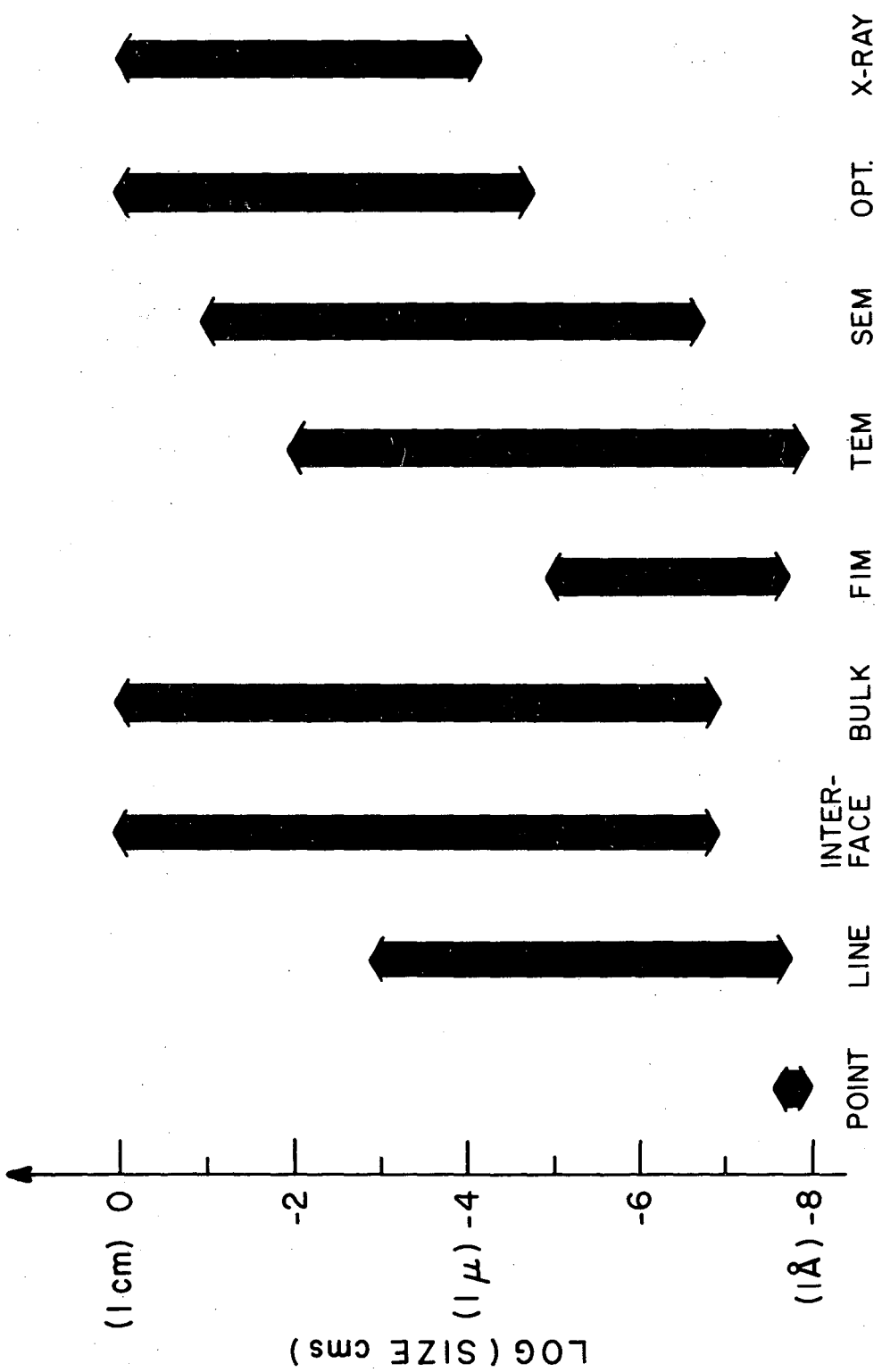

XBL 759-8079

Fig. 1

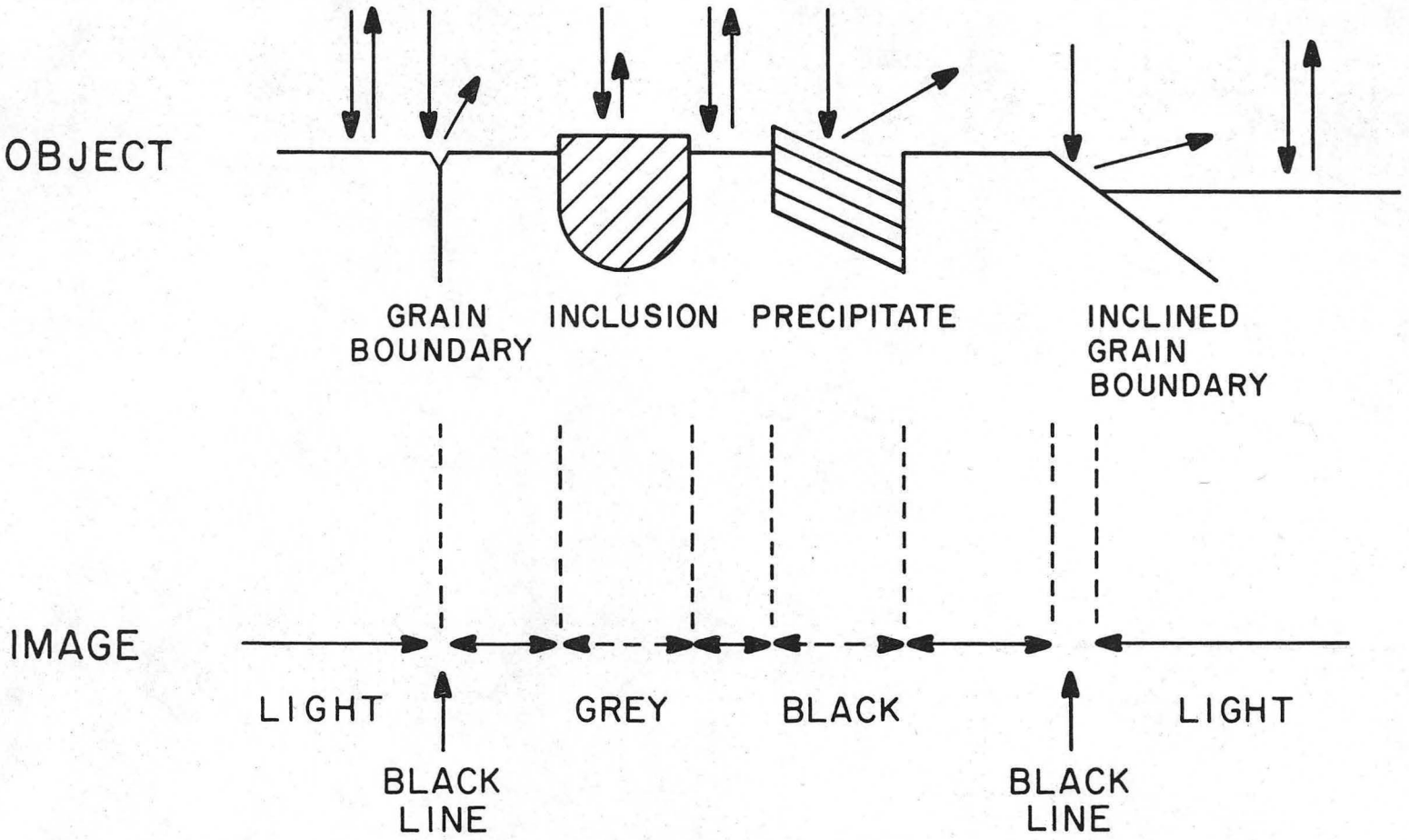

XBL 759-8078

Fig. 2

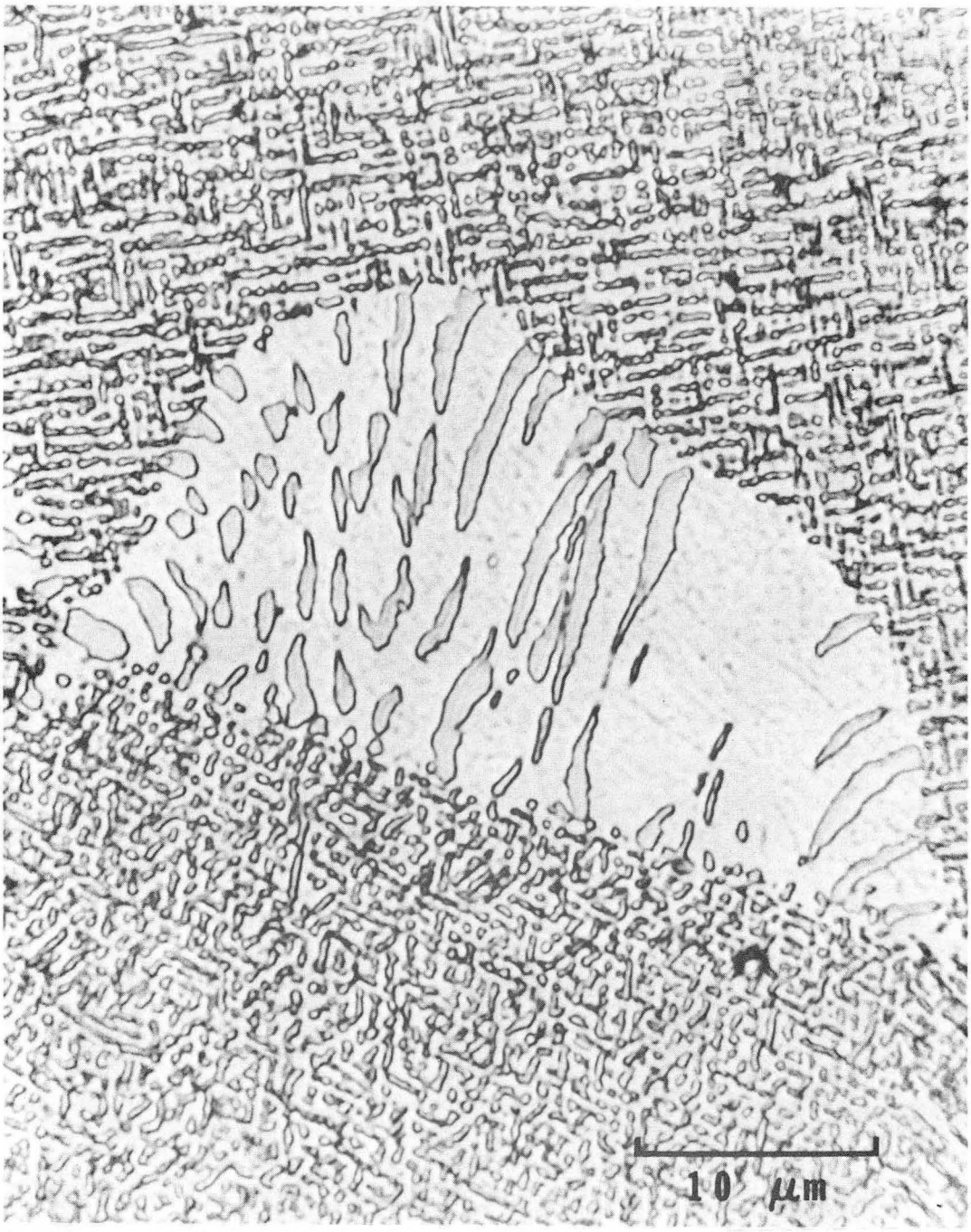

XBB 739-5431

Fig. 3

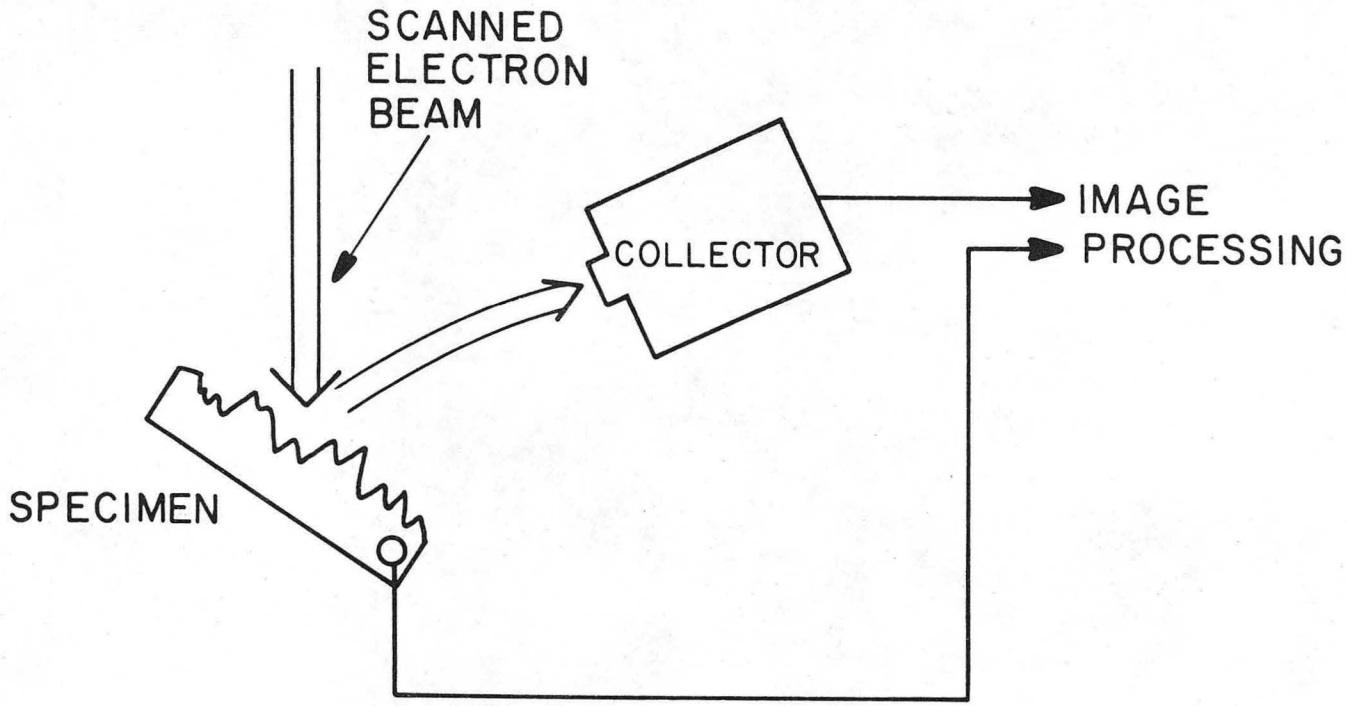

XBL 759-8081

Fig. 4

XBB 759-6529

Fig. 5

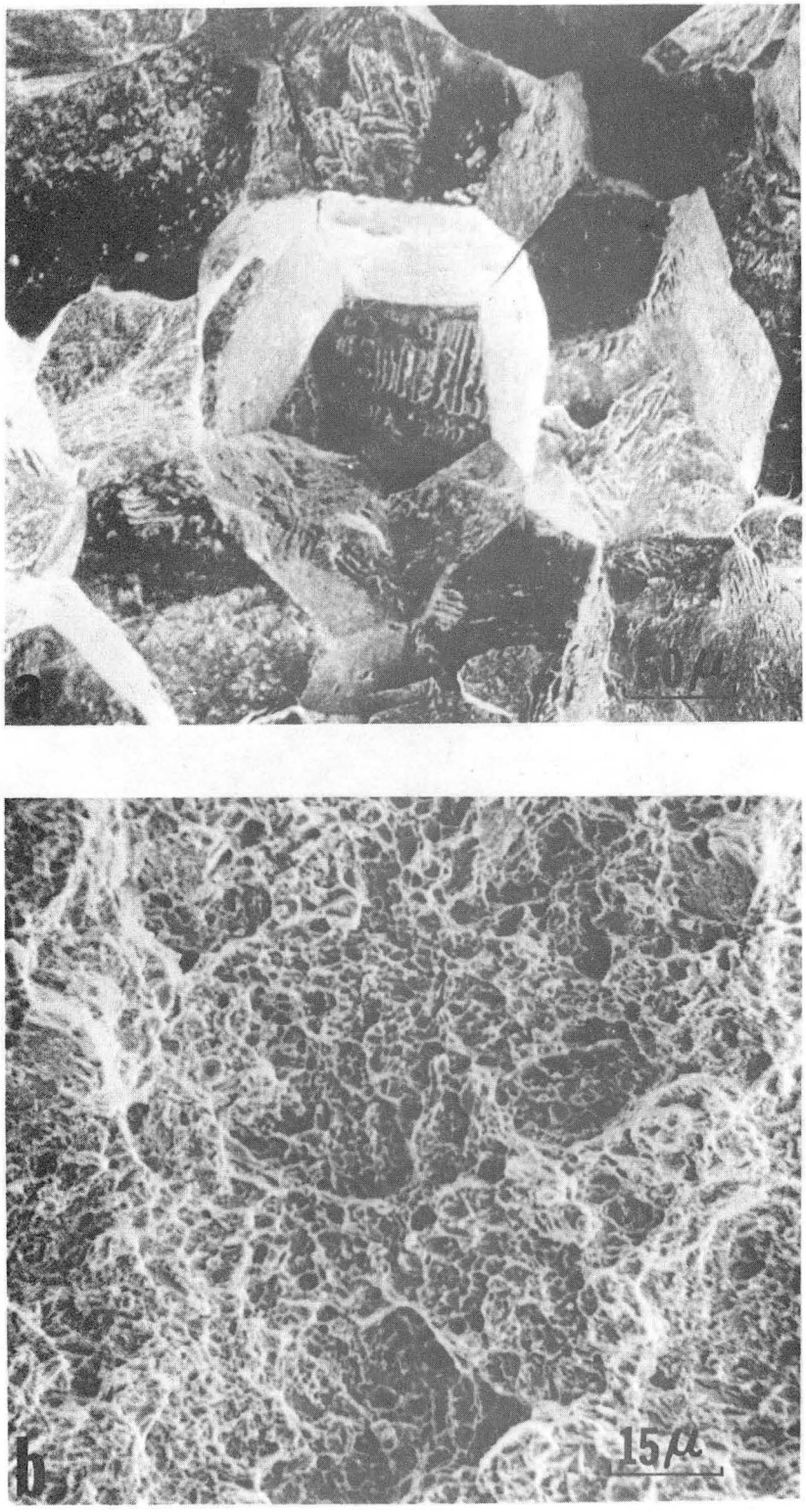

XBB 759-6932

Fig. 6.

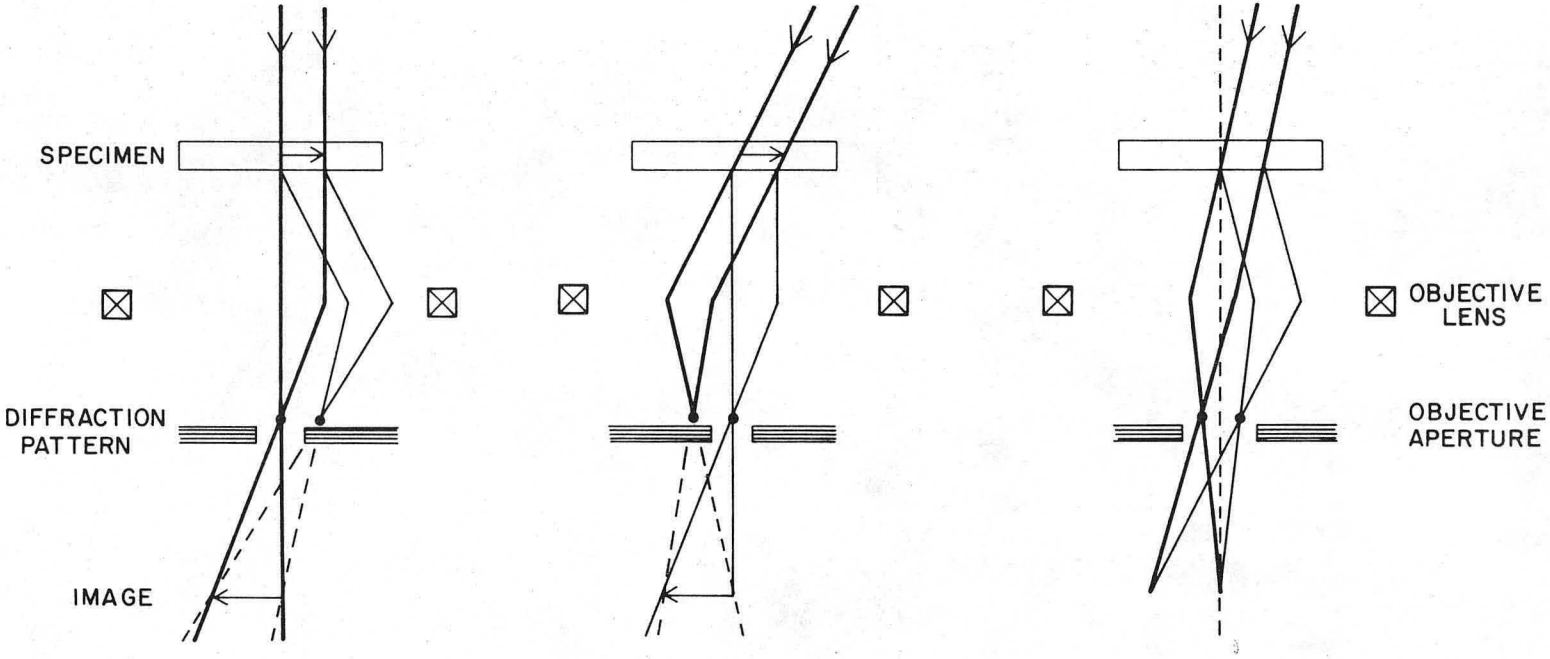

(a) BRIGHT FIELD IMAGE (b) DARK FIELD IMAGE (c) LATTICE IMAGE

XBL 759-8080

Fig. 7

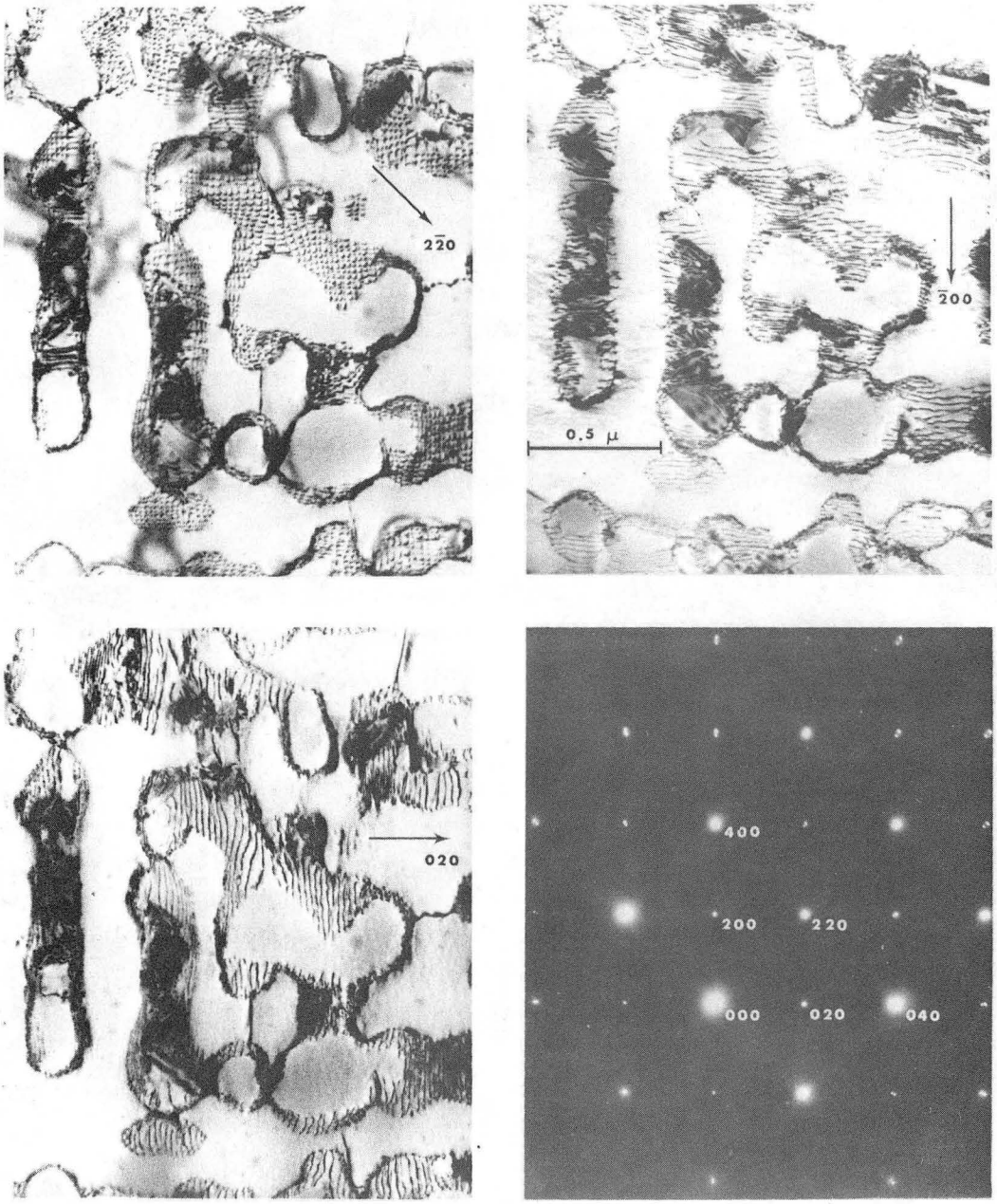

XBB 718-3544

Fig. 8

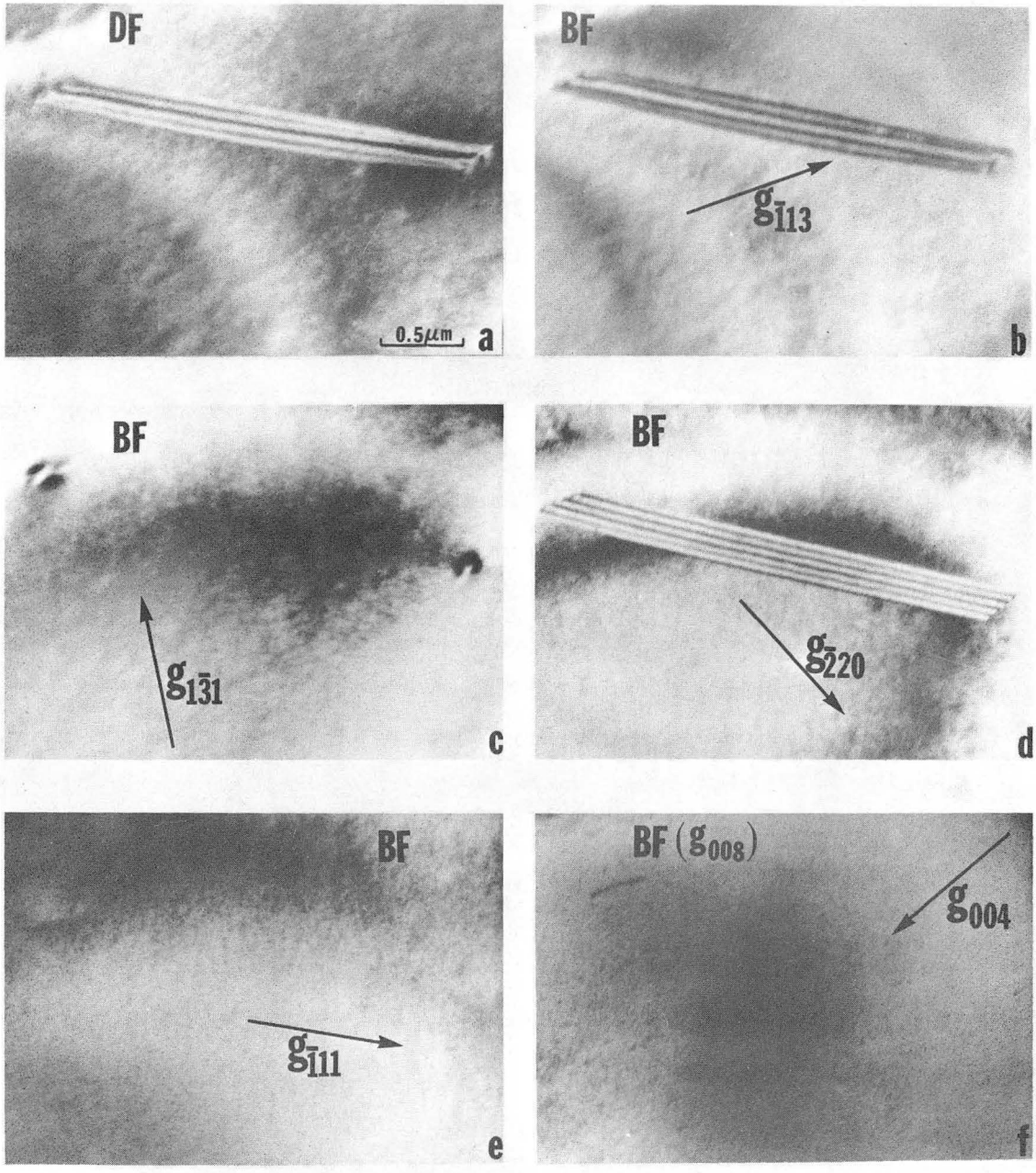

XBB 759-6526

Fig. 9

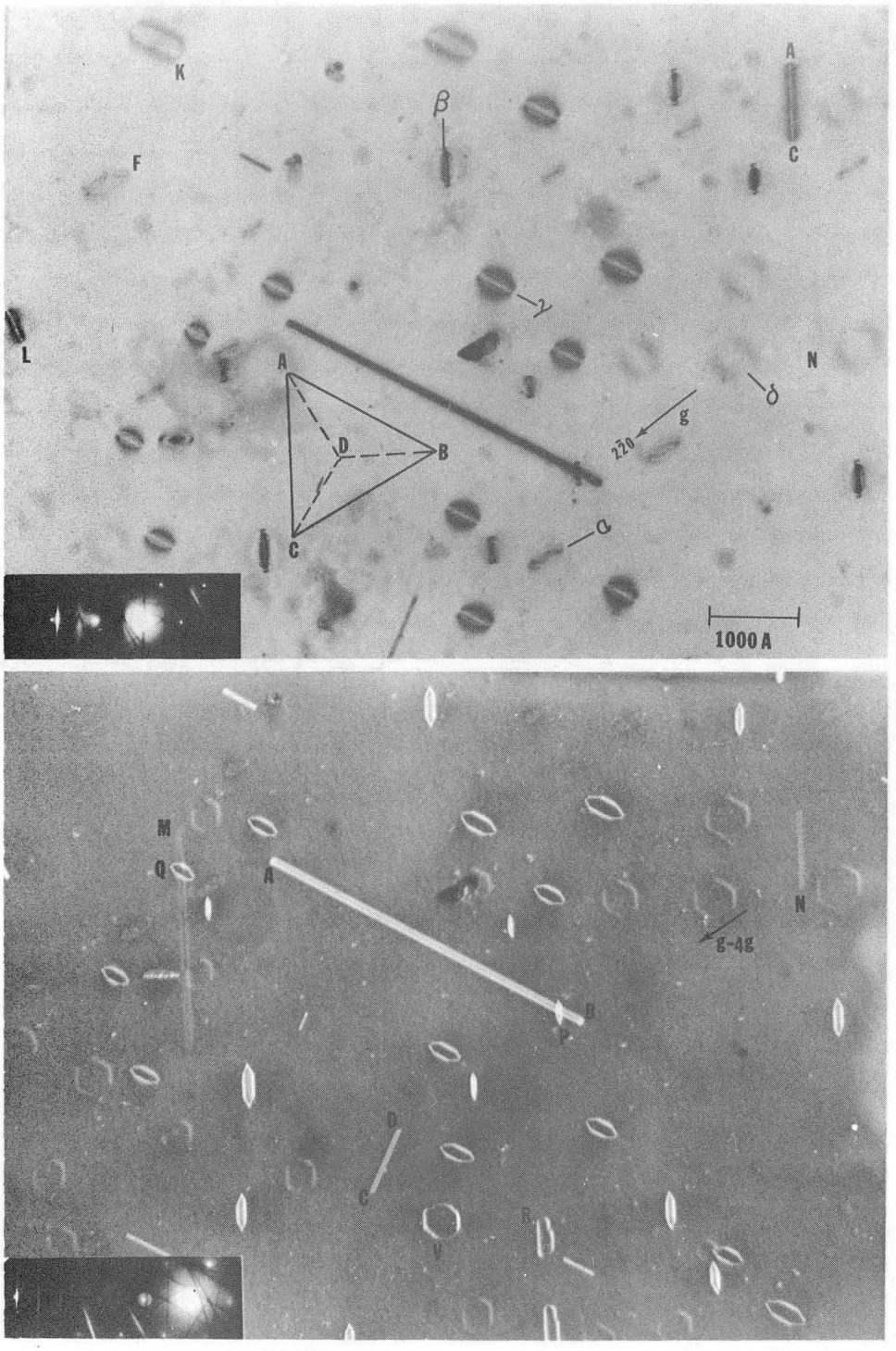

XBB 747-4425

Fig. 10

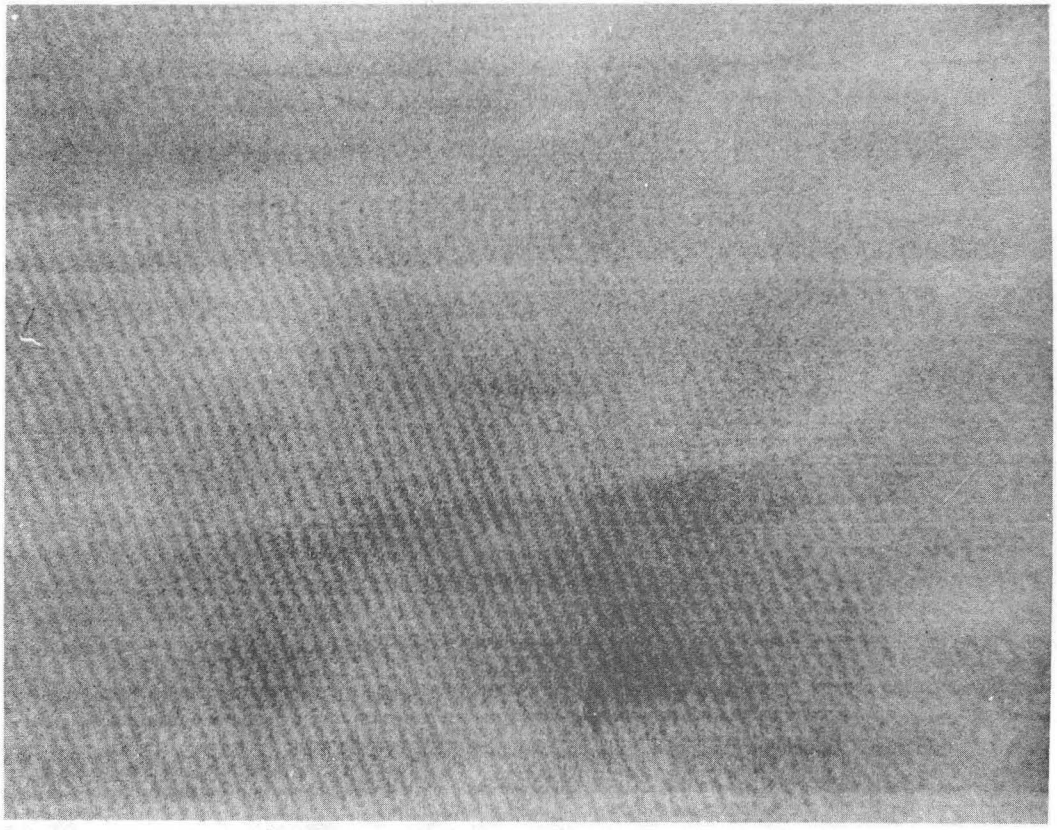

XBB 761-255

Fig. 11

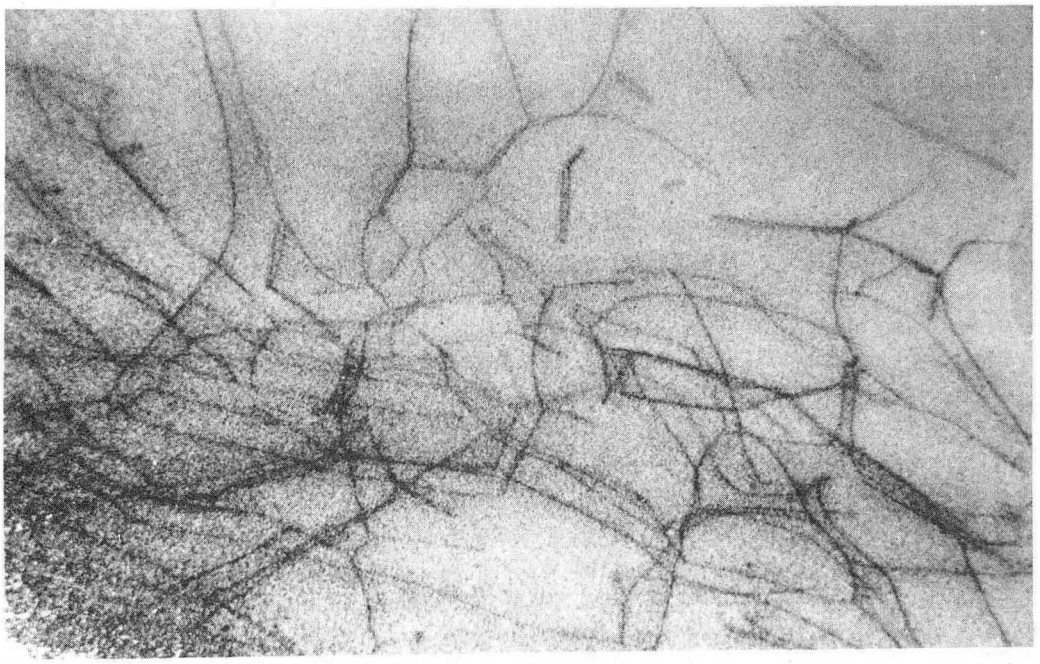

XBB 761-256

Fig. 12

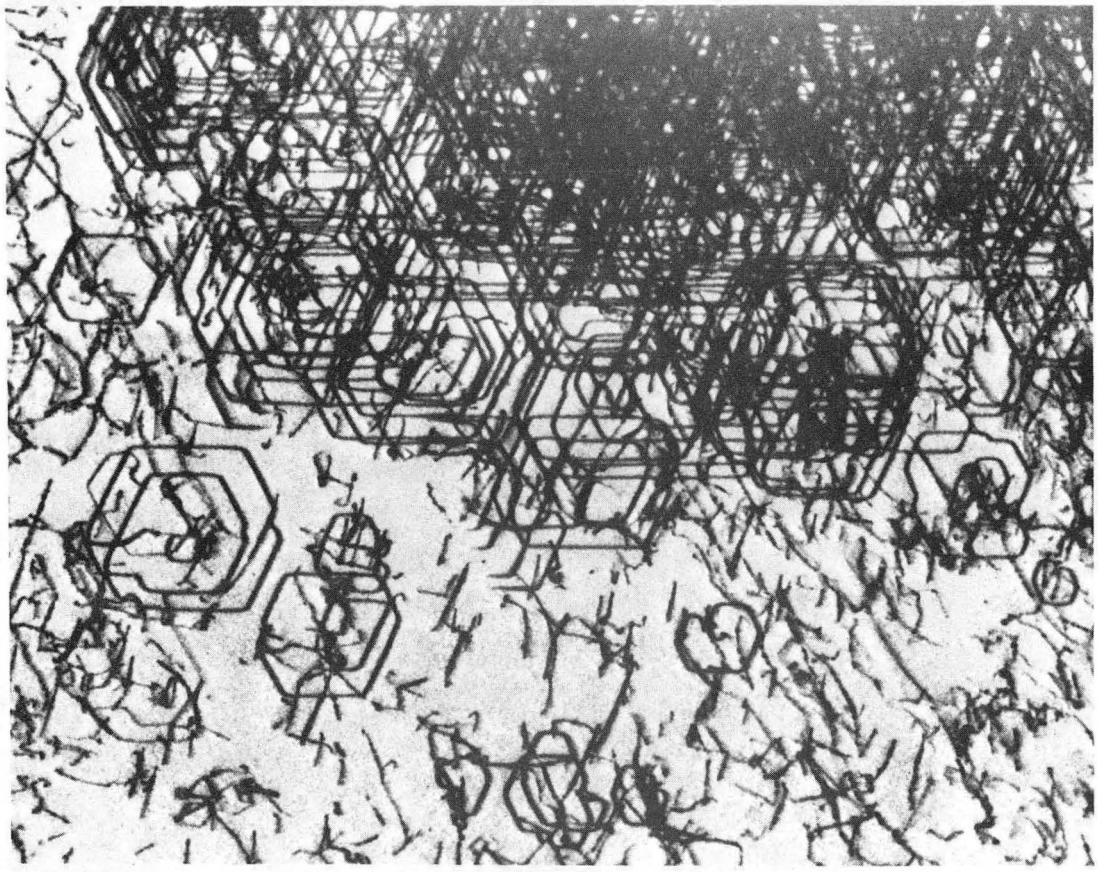

500 μ

XBB 7510-7638

Fig. 13

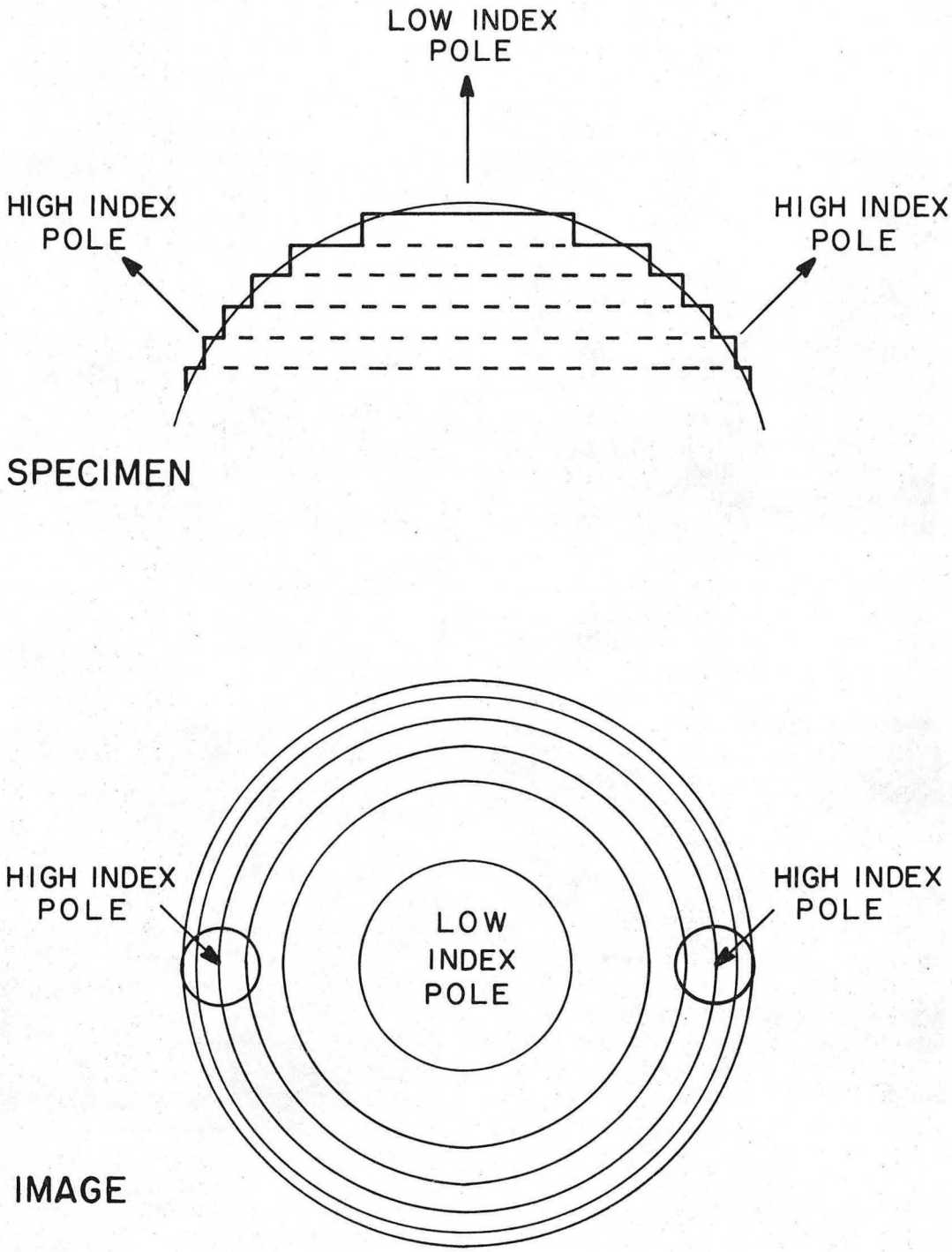

XBL 759-8082

Fig. 14

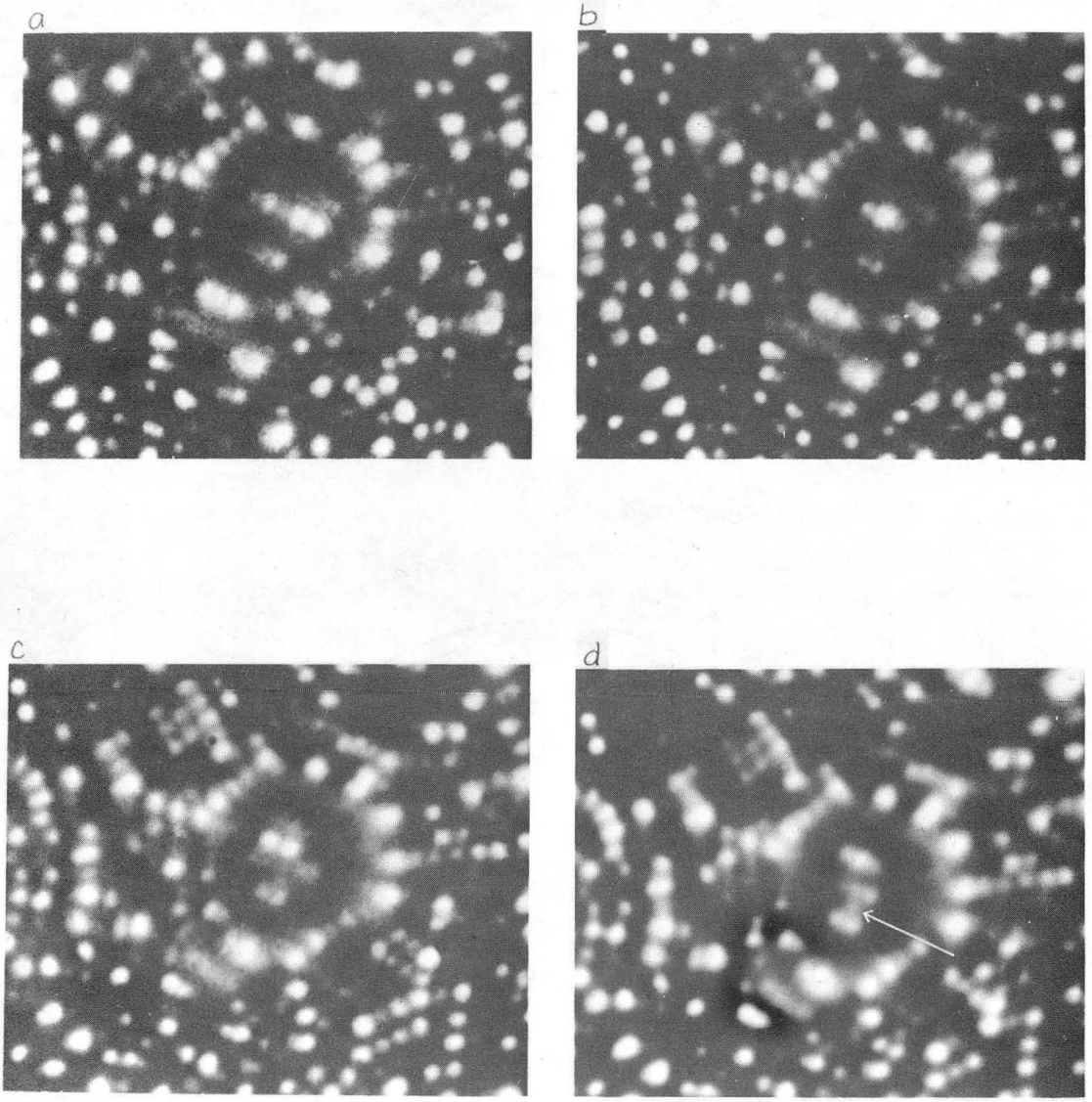

XBB 759-6524

Fig. 15

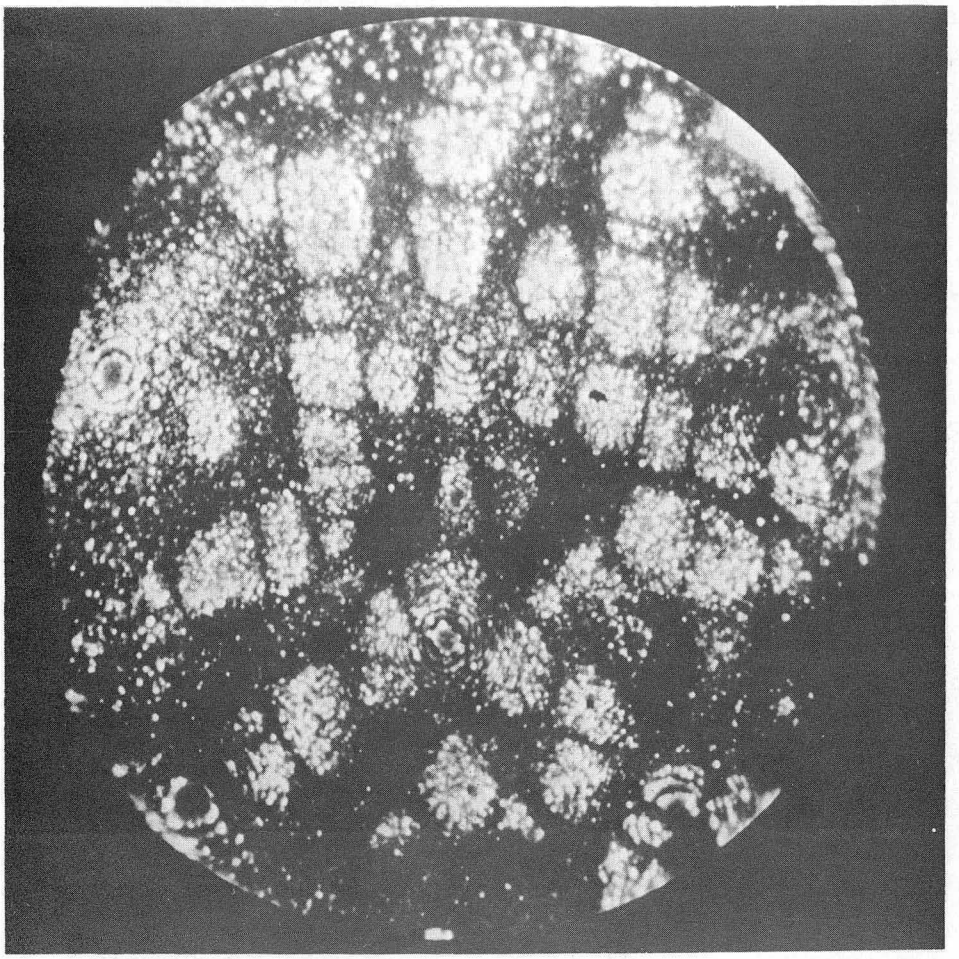

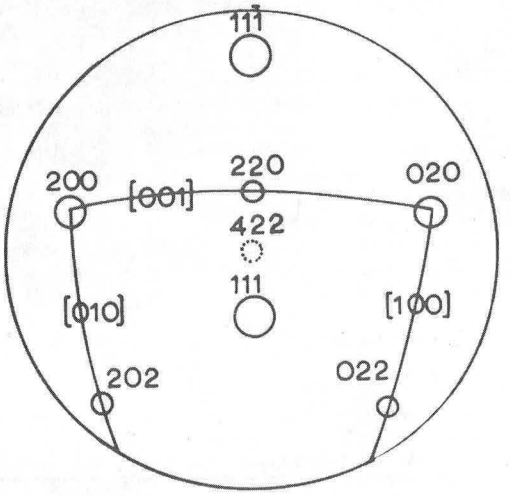

XBB 759-6525

Fig. 16

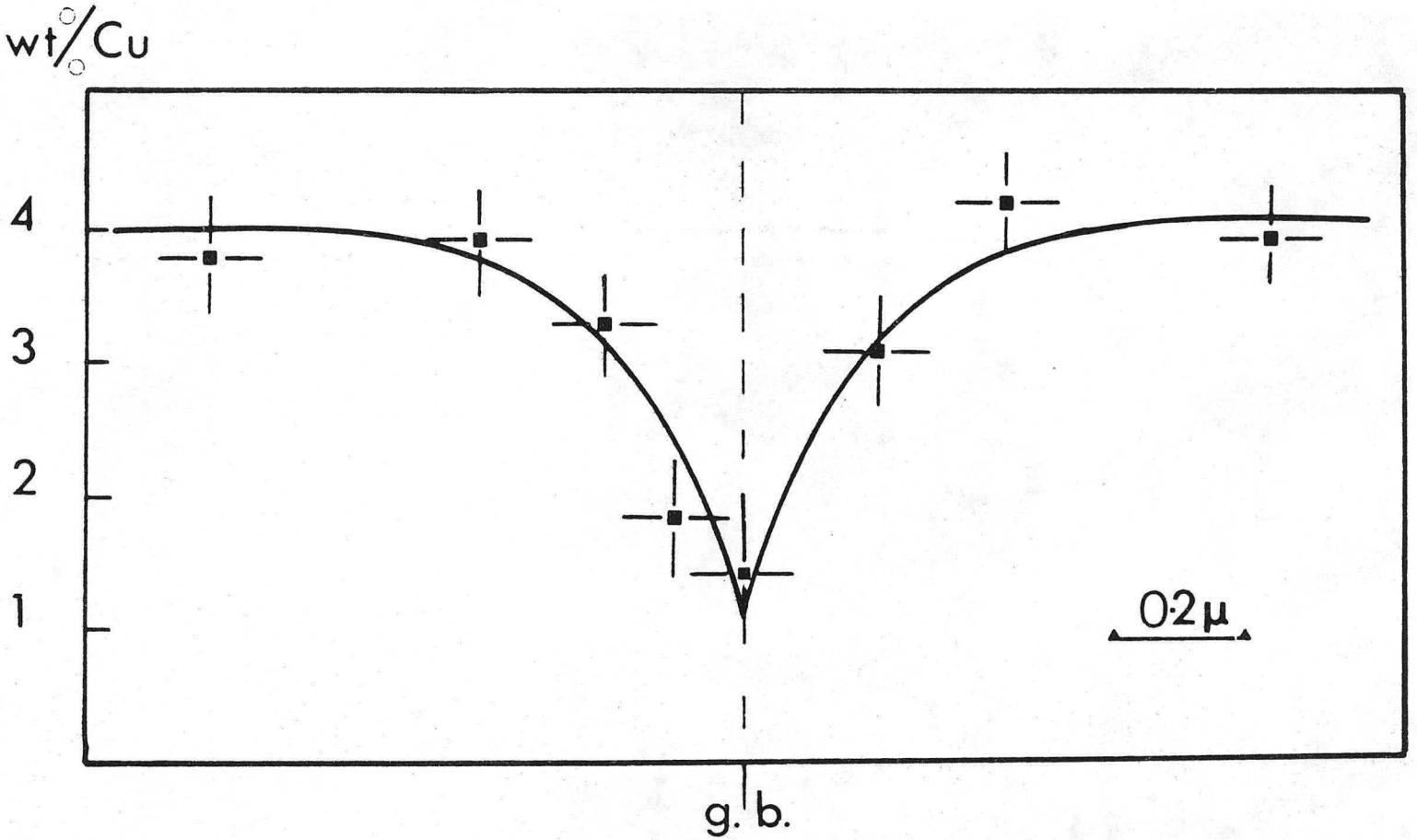

(*b*)

XBL 759-8064

Fig. 17

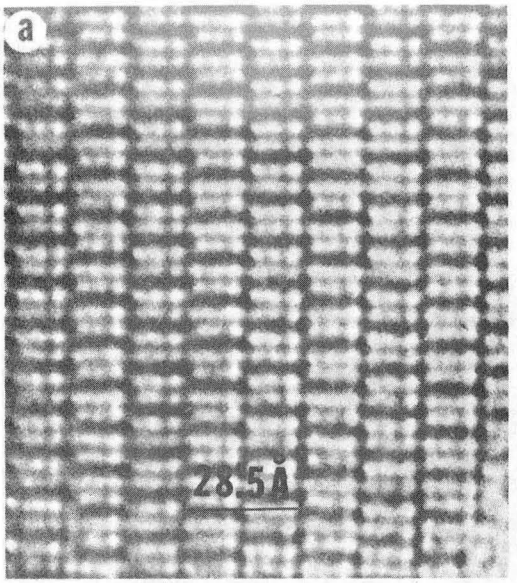

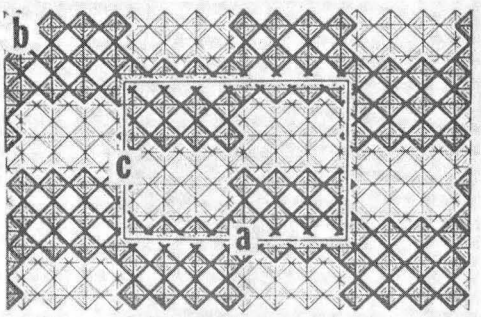

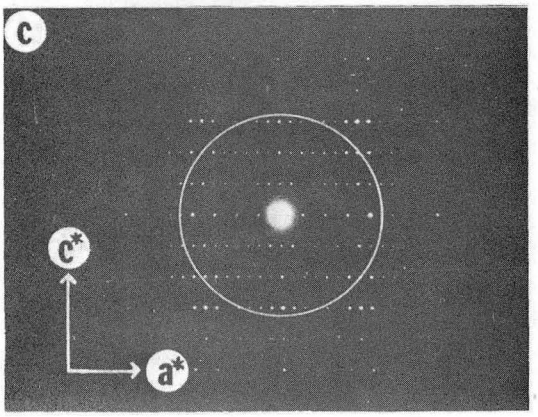

XBB 7510-7902

Fig. 18 (a-c)

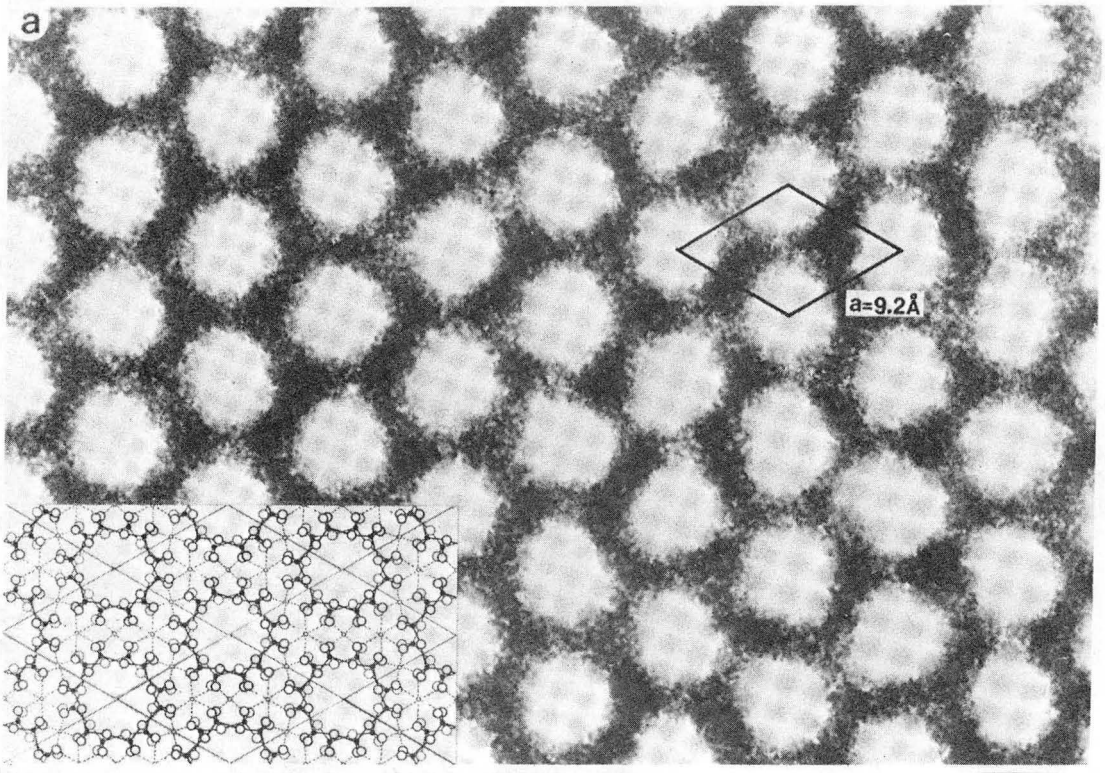

XBB 7510-7641

Fig. 18(d)

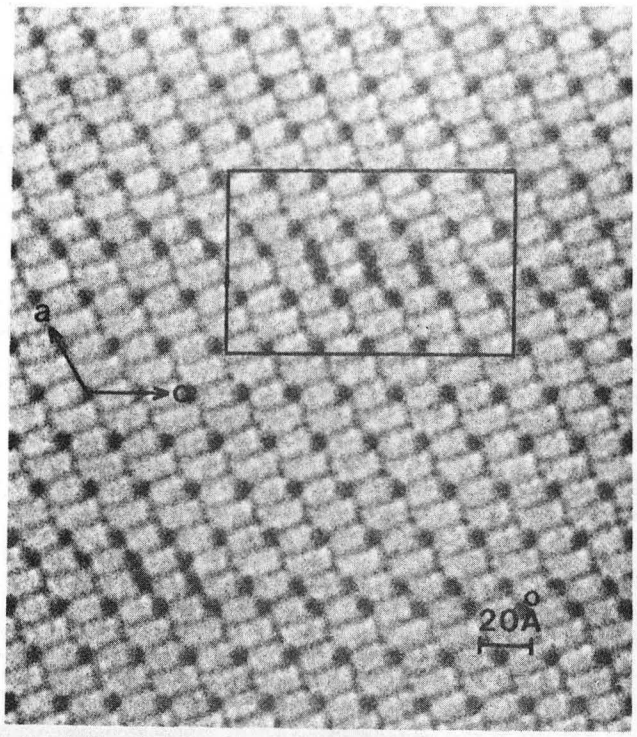

(a)

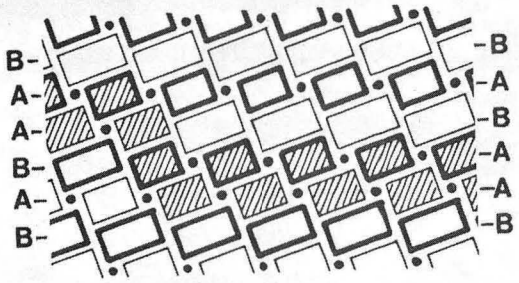

(b)

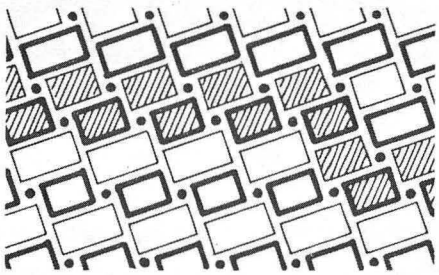

(c)

XBB 7510-7639

Fig. 19

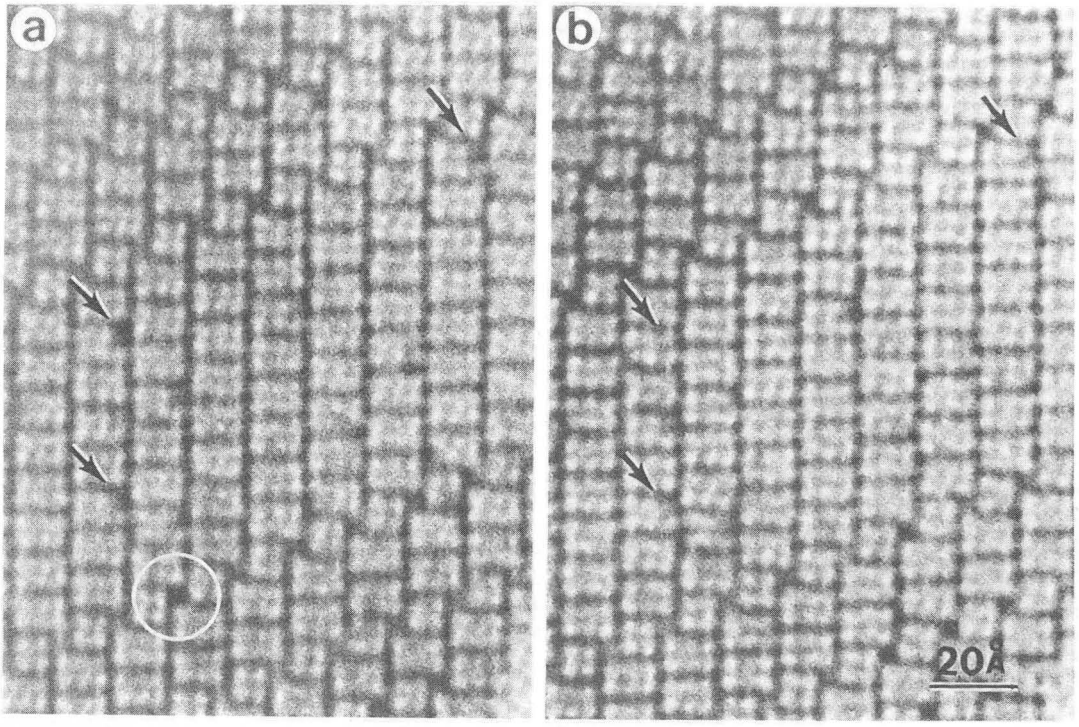

XBB 7510-7636

Fig. 20 (a-b)

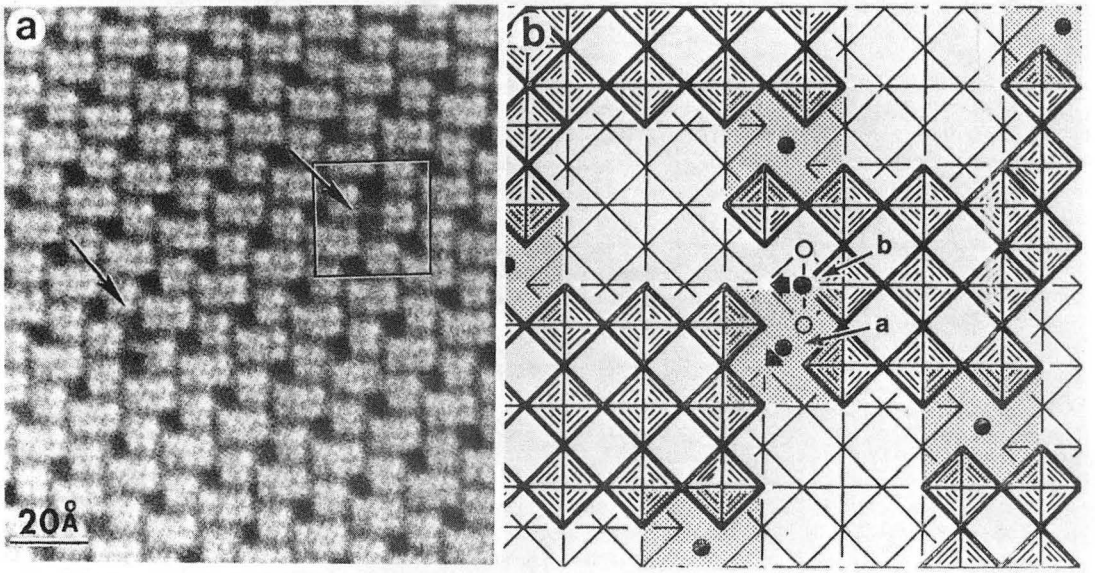

XBB 7510-7637

Fig. 20 (c-d)

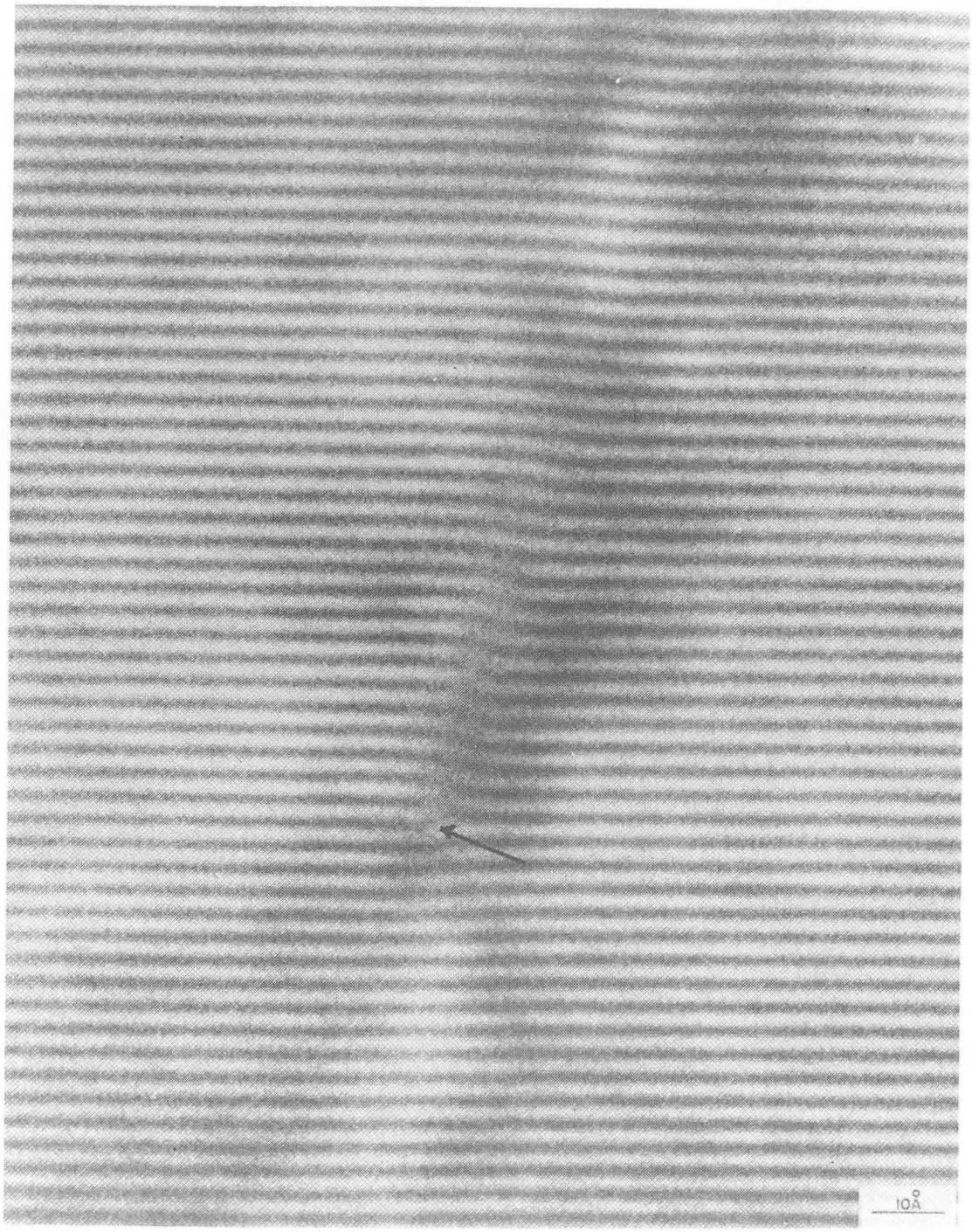

XBB 759-6527

Fig. 21 (a)

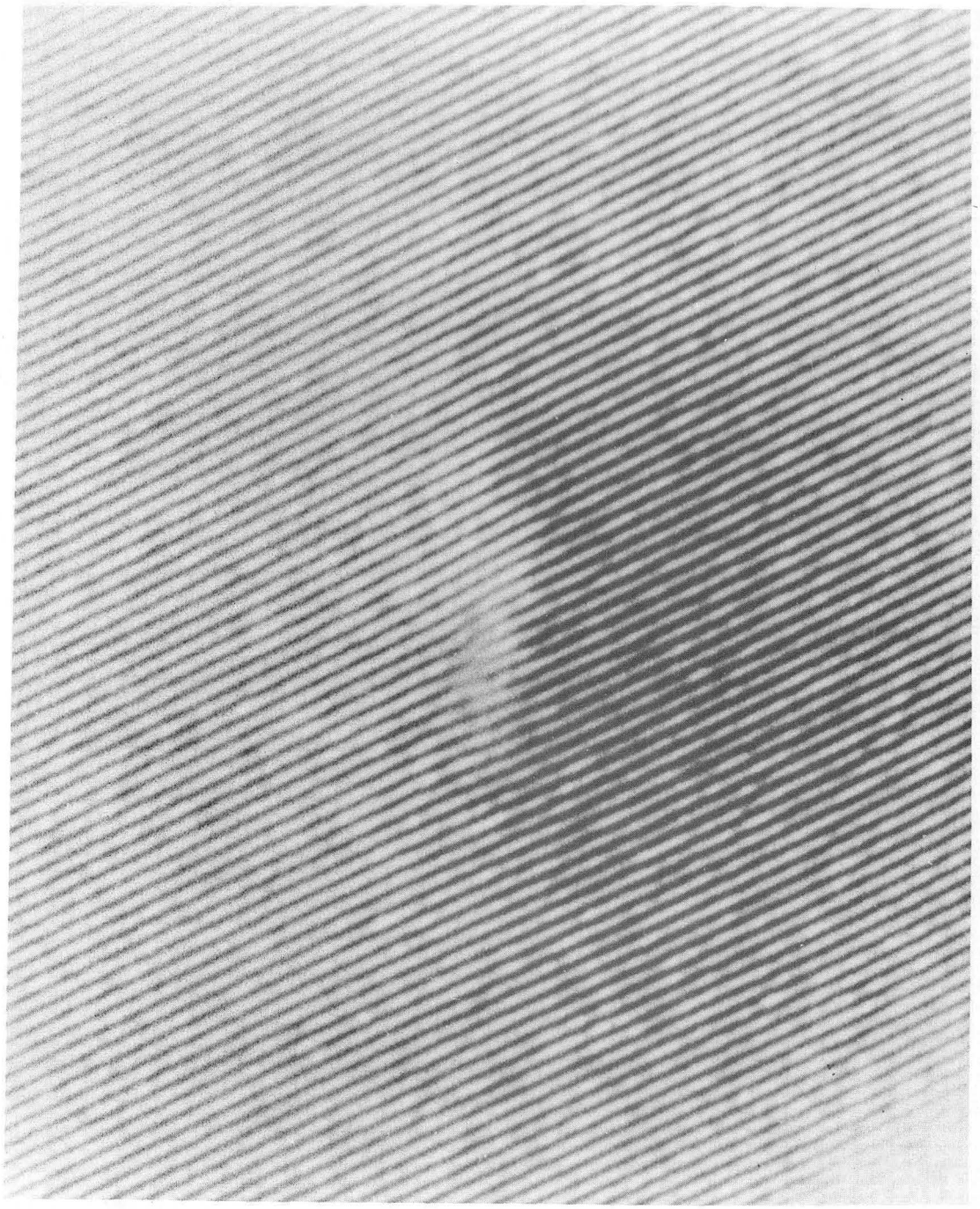

XBB 7510-7768

Fig. 21 (b)

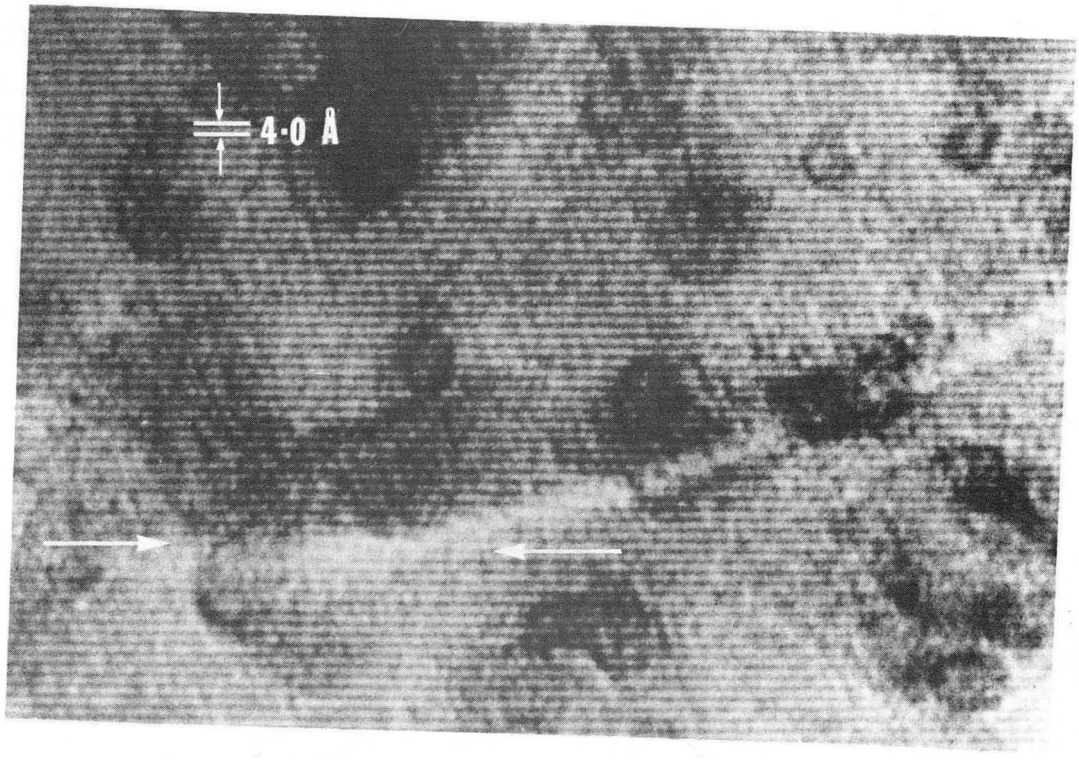

XBB 7410-7097

Fig. 22(a)

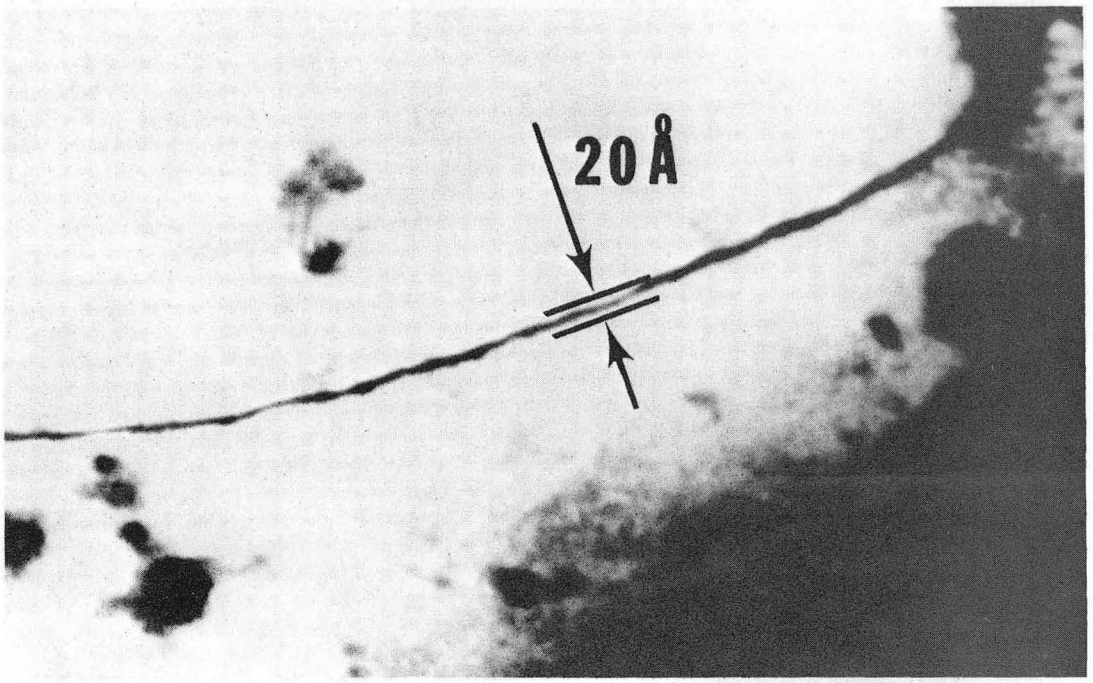

XBB 7412-8987

Fig. 22(b)

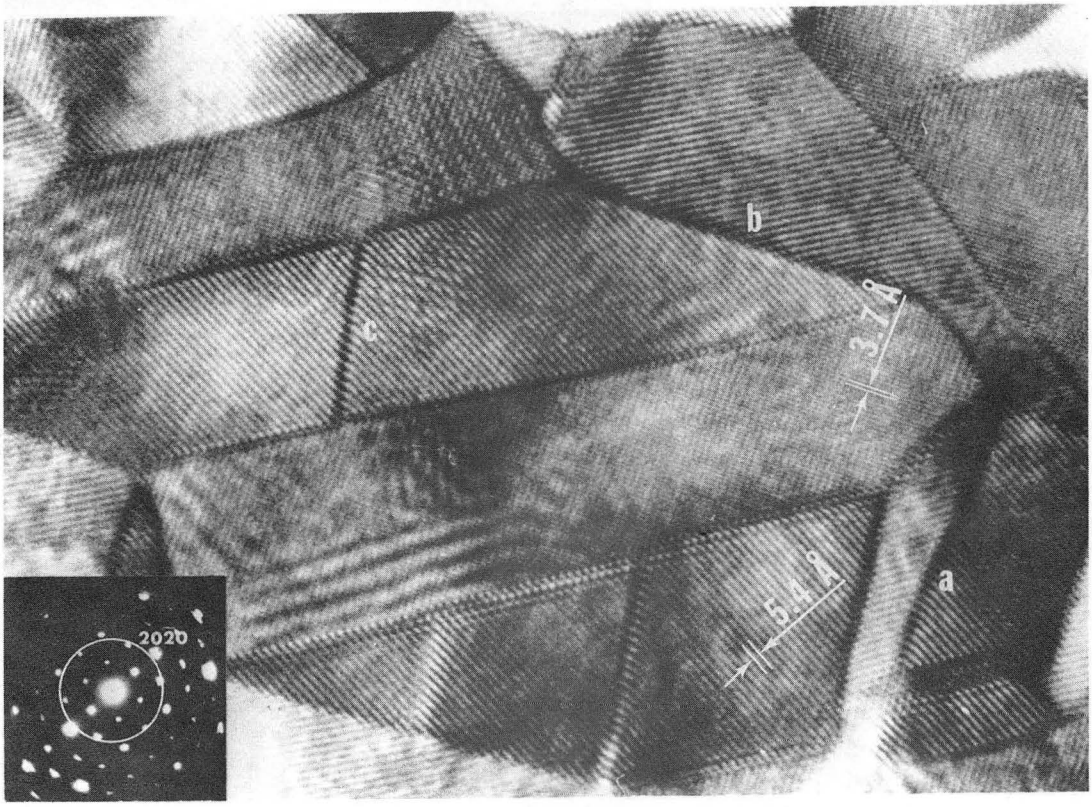

XBB 753-1887

Fig. 23

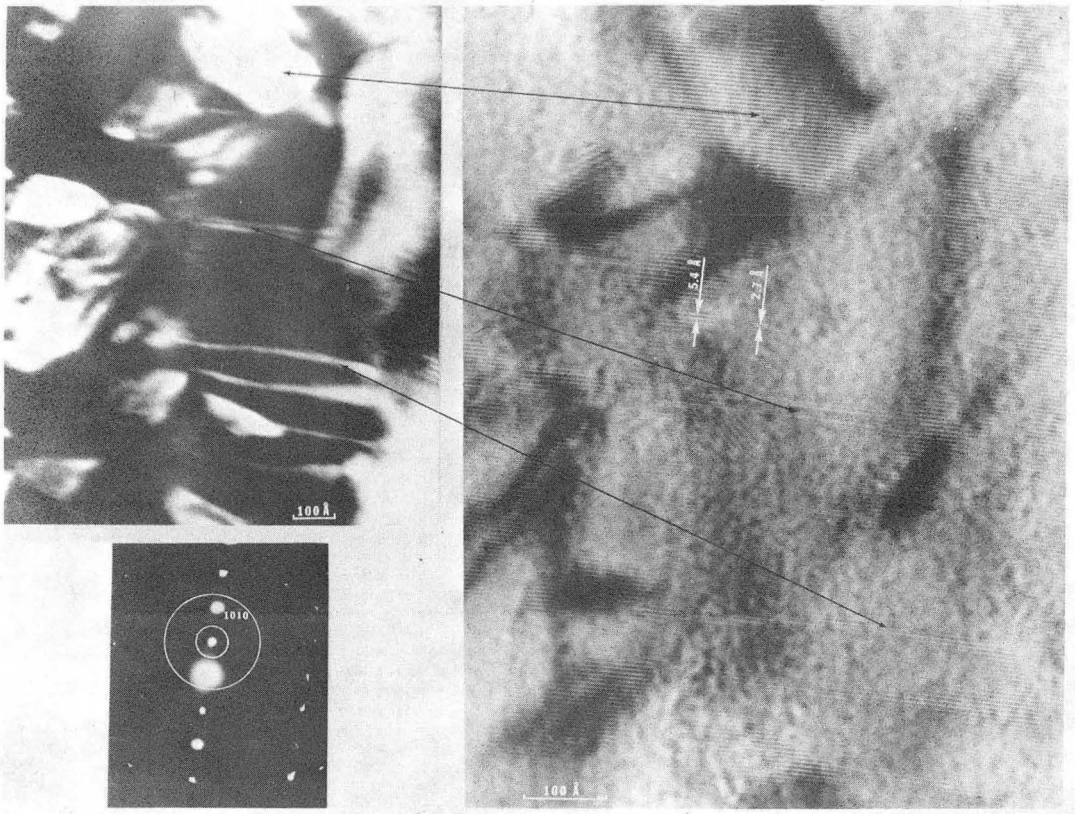

XBB 747-5203

Fig. 24

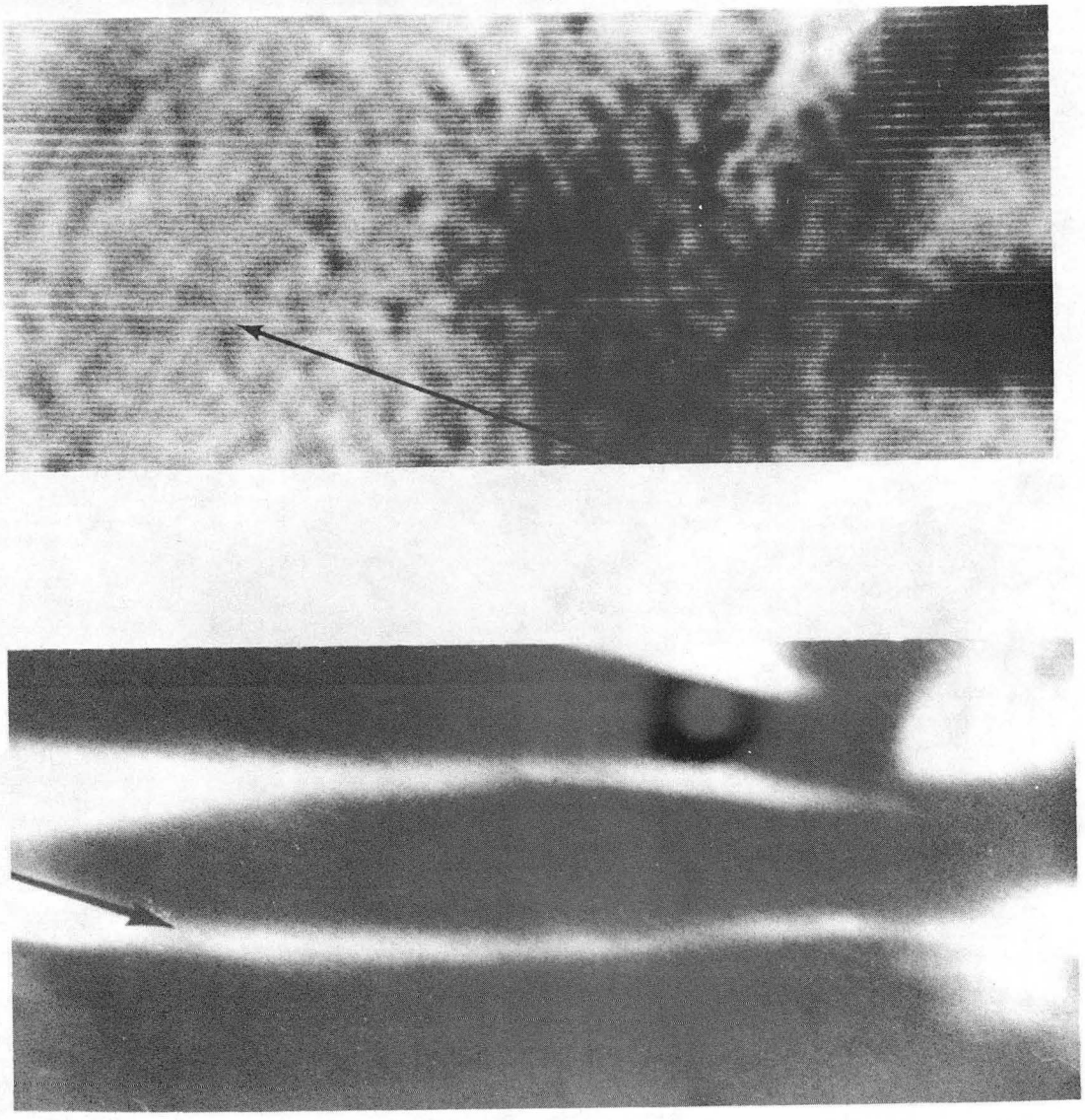

XBB 757-5188

Fig. 25

TECHNICAL INFORMATION DIVISION
LAWRENCE BERKELEY LABORATORY
UNIVERSITY OF CALIFORNIA
BERKELEY, CALIFORNIA 94720